Malaysian Journal of Catalysis
http://mjcat.utm.my/
MJCat
Research Article

Green Synthesis of ZnO Nanoparticles for Kinetics and Thermodynamics Studies of the Photocatalytic Degradation of Selected Dyes under UV Light Irradiation

K. S Kabo[1], A. Yusha'u[1*], S. A. Adabara[1] and H. Abdullahi[2]

[1]*Department of Chemistry, Faculty of Physical Sciences, Federal University, Dutsin-Ma, P.M.B 5001, Katsina State, Nigeria*
[2]*Department of Industrial Chemistry, Faculty of Physical Sciences, Federal University, Dutsin-Ma, P.M.B 5001, Katsina State, Nigeria*

[*]*Corresponding Author: Tel: +123 9026265322 (ayushau21@fudutsinma.edu.ng/auwalyushau2018@gmail.com)*

Article history:
Received 10 March 2026
Accepted 1 June 2026

ABSTRACT

This work presents a biosynthesis of zinc oxide nanoparticle (ZnO NPs) from the *Vigna unguiculata L* extract via co-precipitation method. The prepared photocatlyst was characterized using thermogravimetric differential thermal analysis (TG-DTA), Bruneur-Emmett-Teller (BET), X-ray diffraction (XRD), ultraviolet-visible (UV/Vis), Fourier transform infra-red (FT-IR) and energy dispersive x-ray fluorescence (EDXRF) analyses.TG-DTA results revealed that the calcination temperature was found to be 600 ℃. BET specific surface area was 190.04 m^2g^{-1}. The average crystallite size and band gap values were 50.10 nm and 3.25 eV, respectively. FT-IR analysis demonstrated that the vibrational absorption band of 637 cm^{-1} corresponds to the Zn-O bond. EDXRF result confirmed the presence of Zn and O atoms in the ZnO. The optimal degradation efficiencies of 98.05 & 97.51, 96.58 & 95.65, 96.45 & 94.98 and 96.75 & 93.25 % were achieved at 10.00 mg/L eriochrome black t (EBT)/ methylene blue (MB) initial concentrations, 1.50 g/L ZnO dosage, initial pH of 9.00 and 50.00 ℃ initial temperature in 120.00 min irradiation time respectively. The photocatalytic removal of EBT and MB over ZnO NPs was followed pseudo-first order kinetics with apparent rate constant of 5.33 x 10^{-2} and 4.91 x 10^{-2} s^{-1}, respectively. Activation energy (E_a), enthalpy change (ΔH), entropy change (ΔS) and Gibbs free energy change (ΔG) were + 8.94 & + 14.65 k J mol^{-1}, + 6.27 & + 12.02 k J mol^{-1}, - 82.86 & - 61.56 J $mol^{-1}K^{-1}$ and + 31.37 & + 30.67 k J mol^{-1} for the photocatalytic removal of EBT and MB, respectively

Keywords: *Biosynthesis, Vigna unguiculata L extract, Zinc oxide, Eriochrome black t, Methylene blue and Thermodynamic functions*

| eISSN 0128-2581 |

1. INTRODUCTION

Bio-nanotechnology is a one of the forefront and promising technology that attracted the interest of many scholars, researchers, and engineers due to its wide applications in biomedical, photocatalysis, energy conversion, solar cells and food processing in the world [1-4]. This technology also known as green nanotechnology and it involves the production of nanoparticles usually ranging from the 1.00-100.00 nm from the extract of biological sources [5, 6]. Some of the common examples of nanoparticles include ZnO, TiO_2, CuO, ZrO_2, WO_3, Cu_2O, Fe_2O_3, ZnS, ZrS, SrO_2, CuS, and ZTO [7-12]. Today, zinc oxide nanoparticles (ZnO NPs) have been recognized as one of the promising candidate for photocatalytic applications due to its chemical stability, non-toxic, low cost, environmental friendly species, highest conversion efficiency, photocatalytic performance and physicochemical properties as compared to the abovementioned counterpart photoresponsive nanoparticles [13-16]. On the other hand, the synthesis of ZnO NPs has been reported by the different physical and chemical approaches such as sol-gel, solvothermal, thermal evaporation, hydrothermal, mechanochemical, precipitation, co-precipitation, sputtering oxidation, micro-emulsion, chemical vapor dispersion, electroplating, atomic layer decomposition, anodic oxidation and green methods [17-20]. The conventional methods for preparation of ZnO NPs used harmful chemicals, high energy consumption, and generate hazardous byproducts, rising environmental problems and health concerns [21].

Recently, a green approach has been considered as a beautiful and reliable alternative method for the synthesizing ZnO NPs [22]. Green synthesis is also called biosynthesis and it involves the use of plant extracts, fungi, and bacteria to develop nanomaterial formation [23]. Many literatures demonstrated that among the various biological resources, plant extracts are preferred for green synthesis because of their availability, low cost, friendly species and rich content of bioactive compounds which act as capping, reducing and stabilizing agents [24]. *Vigna unguiculata L* (bean leave) is

a widely cultivated leguminous plant that contains polyphenols and antioxidants, making it an excellent candidate for green synthesis of ZnO NPs. Moreover, *Vigna unguiculata L* extract was used in this study due to its availability, low cost, having self-fertilizer and growth fast in comparison with other plant extracts [25]. Additionally, the use of *Vigna unguiculata L* extract not only elevates an environmentally friendly synthesis route but also enhances the photocatalytic performance for the prepared ZnO NPs, potentially increasing their applications in photocatalysis [26].

However, the photocatalytic activities for the biosynthesized ZnO NPs were evaluated using EBT and MB dyes as model substrates. EBT is an anionic dye that belonging to anionic-azo-group of organic dyes while MB is a cationic dye that belonging to cationic-azo-organic dyes. Both the EBT and MB dyes are extensively used in the textile, paper, leather, ceramic, paints, rubber and pharmaceutical industries as the coloring materials of their final products [27, 28]. These industries however, discharged their effluents directly into the aqueous environment without proper treatment. Many literatures reported that about 17.00-20.00 % of industrial water pollutions were caused by the dyeing process in which EBT and MB have been listed among the priority pollutants [29]. Various wastewater treatment methods like precipitation, distillation, filtration, adsorption, biodegradation, reverse osmosis, ultra-filtration, and decantation for the removal of EBT and MB dyes have recorded and insignificant responses were obtained [30-35] due to high solubility in water, large molecular weight and stability of EBT and MB dyes [36]. Secondly, most of these classical methods abovementioned were expensive, time consuming and required extra planning [36].

Nowadays, heterogeneous photocatalysis has been recognized as an excellent technology used for the photodegradation of EBT and MB dyes due its advantages such as absence of sludge, secondary pollutants, and conversion of recalcitrant into environmentally friendly carbon dioxide (CO_2) and water (H_2O) over than the conventional methods [37]. This technology however, involves the use of holes and hydroxyl radical significantly harvested from the light excited photoresponsive catalyst [38]. Today, the photocatalytic of degradation of EBT and MB dye have been extensively investigated by many scholars and researchers. For instance, Yusha'u *et al* [39] reported the sol-gel synthesis of ZnO NPs for optimized photocatalytic degradation of EBT under UV light irradiation. The optimum photodegradation efficiency of 96.59 % was obtained at 15. 00 mg/L of EBT dye, 0.40 g/L catalyst dosage and initial pH of 9.00. Auwal and Gaya [40] investigated the mechanochemical synthesis of C-doped ZnO NPs for enhanced photocatalytic degradation of EBT dye. The optimum degradation efficiency of 97.00 % was achieved at 5.00 mg/L of EBT dye, 0.10 g/L C-doped ZnO and pH of 11.00 using face central composite design (FCCD) of the response surface methodology (RSM). Similarly, Yusha'u *et al* [41] studied the visible light induced photocatalytic removal of MB using Cu-tunable *p*-type ZnO NPs. The optimum photodegradation efficiency of 98.00 % was found at 0.30 g/L catalyst dosage, 10.00 mg/L initial MB dye concentration and initial pH of 6.00. The degradation model was statistically remarkable with $p <$ 0.0001 % in which the MB initial concentration and solution pH were the most significant variables influencing the removal of MB over Cu tunable *p*-type ZnO photocatalyst under visible light irradiation. The photocatalytic degradation of MB using the undoped and Cu-doped ZnO NPs followed pseudo-first kinetics scheme.

Accordingly, Khan *et al* [42] reported the green synthesis of ZnO NPs using peels of *Passiflora foetida* extract for the degradation of hazardous organic dyes. The ZnO NPs exhibit excellent degradation efficiency towards organic pollutant dyes, i.e., Methylene blue (93.25 % removal) and Rhodamine B (RhB) (91.06 % removal) in 70.00 min, under natural sunlight with apparent rate constant 0.0337 min^{-1} (R^2 = 0.9749) and 0.0347 min^{-1} (R^2 = 0.9026) respectıvely. Additionally, Setyarsih *et al* [43] investigated the green synthesis of ZnO NPs from *Pineapple skin* for photodegradation of congo red (CR) dye. The effectiveness of the photodegradation of the synthesized ZnO NPs was altered by the mass of the catalyst under the duration of UV light irradiation. Catalyst masses of 5.00, 8.00, 10.00, 12.00, 20.00 and 30.00 mg were able to degrade CR dye with a concentration of 30.00 ppm, respectively 93.51, 93.87, 95.15, 96.15, 97.72 and 97.08 % after irradiation for 210.00 min. With the large percentage of CR dye photodegradation, the ZnO NPs resulting from the research showed good photocatalytic activity. In another work separately, Alprol *et al* [44] recorded the green synthesis of ZnO NPs using *Padina pavonica* extract for efficient photocatalytic degradation of methylene blue. The synthesized NPs, characterized by Fourier transform infrared (FT-IR) spectroscopy, scanning electron microscopy (SEM), energy dispersive x-ray (EDX) spectroscopy and zeta potential, demonstrated high adsorption capacity (Q_m = 192.308 mg g^{-1}) and excellent removal efficiency (> 98.00 %) for MB at low concentrations. Langmuir isotherm and pseudo-second order kinetic models best fit the experimental data., suggesting monolayer adsorption and chemisorption as the primary mechanisms. Moreover, Kahsay *et al* [45] studied the green synthesis of ZnO nanostructures from *Dolichos lablab L* extract for photocatalytic and bactericidal applications. The results showed the highest efficiency of photodegradation of ZnO nanostructures for methylene blue (MB) (80.00 %), rhodamine B (RhB) (95.00 %) and orange II (O II) (66.00 %) at pH values of 11.00, 9.00 and 5.00 respectively, in 210.00 min time interval. In addition, the antimicrobial activity of ZnO nanostructures using the agar well diffusion method against *Bacillus pumilus* and *Spingomonas paucimobilis* showed the highest zones of inhibition of 18.00 mm and 20.00 mm, respectively. Hence, ZnO nanostructures have the potential to be used as a photocatalyst and bactericidal component.

Despite the coexisting works available in the scientific literatures, the green synthesis of ZnO NPs from *Vigna unguiculata L* extracts has not been previously investigated. Secondly, the thermodynamic investigation for decomposition processes during the biosynthesis of ZnO NPs from *Vigna unguiculata L* extract has not been investigated previously. Additionally, the kinetics and thermodynamics studies of the photocatalytic degradation of EBT and MB over the biosynthesized ZnO NPs from *Vigna unguiculata L* extract also have not been reported previously in the existing literatures. Therefore, this work aimed to study the green synthesis of ZnO NPs from *Vigna unguiculata L* extract for thermodynamic studies of the photocatalytic degradation of EBT and MB dyes under ultraviolet (UV) light irradiation. Similarly, the effects of primary parameters such as EBT and MB initial concentration, catalyst dosage, initial pH, and initial temperature were investigated. Moreover, the radical scavenger and durability tests were also evaluated. Finally, the results obtained from this work were compared with that of the recent previous related works recorded in the relevant scientific literatures.

2. EXPERIMENTAL

2.1 Materials

All the materials used in this study were used as received from the manufacturer and they are all in analytical grade. These materials include zinc acetate dehydrate ($Zn(CH_3COO)_2$.$2H_2O$, 98 %; Sigma Aldrich), sodium hydroxide (NaOH, 97 %; Merck), dil. hydrochloric acid (HCl, 98 %; Sigma Aldrich), ethanol (C_2H_5OH, 96 %; Merck), butanol (C_4H_9OH, 95 % ; Sigma Aldrich), benzoquinone ($C_6H_4O_2$, 97 %; Merck), ammonium oxalate ($(NH_4)_4C_2O_4$, 98 % ; Merck), deionized water (H_2O, highly pure; Fudma Lab), eriochrome black t ($C_{20}H_{12}N_3N_aO_9S$, 98 %; Sigma Aldrich), methylene blue ($C_{16}H_{18}N_3ClS$, 98 %; Merck) and bean leaves obtained from the Garden Department of Biology Faculty of Life Sciences, Federal University Dutsin-Ma (FUDMA).

2.2 *Vigna unguiculata L* collection and identification

The local and market names of the sample used in this study was bean which is a popular herbaceous annual plant grown and cultivated for edible dry seeds or green and unripe pods. Its leaf is widely used as a vegetable, straw as fodder and functions as a protein in the biological system. This species adopted different environmental conditions due to self-nutritional nature on comparison with the other species of plants. Both the seed and leaves of bean served as a protein and produced higher yields of agricultural products. Bean leaves are more versatile in the aqueous ecosystems due to its self-nutritional properties, ability to adopt different environmental conditions, and higher yields of agricultural products. However, bean leaves were used because it's possessed self-nutrients and fast growing than the other counterpart plants at various surrounding environments. On the other hand the scientific name of bean is called *Vigna unguiculata L.* The *Vigna unguiculata L* was collected from the specific areas (from the east, west, south, north and center point) [44]. The plant specimens were identified at Herbarium of the Botanical Garden of Faculty of Life Science Department of Biology Federal University Dutsin-Ma (FUDMA), Katsina State Nigeria. After the identification by the expert then the samples were thoroughly washed multiple times with tap water, followed by rinsing with deionised water to eliminate any adhering dust, debris or other particulates. After cleaning, the samples were air-dried at room temperature for several hours and then ground into fine a fine paste. The shape of *Vigna unguiculata L* is presented in Figure 1.

Figure 1. Shape of *Vigna unguiculata L*

2.3 Preparation of *Vigna unguiculata L* extract

The procedure reported by Basit *et al* [46] was adopted and modified for the current study. In this method, the fresh leaves of *Vigna unguiculata L* were washed several times with deionized water to remove debris, dust, dirt and suspended particles. Then the leaves were dried in the dark at room temperature (RT) for two (2) weeks. The dried leaves were ground with a mortar and pestle. An amount of 20 g of leaves powder was taken into 500 ml of deionized water and boiled at 60 ^oC for 4 hours through magnetic stirrer at stirring speed of 600 rpm. The resulting extracted solution was allowed to cool and filtered by using Whatman filter paper No. 1. The filtrate was used to prepare ZnO nanoparticles.

2.4 Synthesis of zinc oxide nanoparticles (ZnO NPs)

Green synthesis of ZnO NPS reported by Selim *et al.* [47] and Abegunde *et al* [48] was adopted and altered for the present synthesis via precipitation method. The solution prepared with 20.00 ml of *Vigna unguiculata L* extracts, 80.00 ml of deionized water and 5.93 g of zinc acetate dehydrate ($Zn(CH_3COO)_2{\cdot}2H_2O$) was set-up .Then stirred at temperature 90^oC, constant speed at 500 rpm for 23.00 min and then homogenized for 5 min by constant stirring using magnetic stirrer. Then sodium hydroxide (0.05MNaOH) was added drop wise to the solution till pH 11. The past was formed after continuous heating and stirring then dried overnight in an oven. The resulting powder was evaporated at 80 ^oC for 10 hours and calcined at 600^oC for 2 hours using muffle furnace to obtain ZnO NPs.

2.5 Characterization of ZnO NPs

The synthesized ZnO NPs were subjected for characterization using a powerful analytical techniques such as x-ray diffraction (XRD), ultraviolet-visible (UV-Vis) spectrometry, energy dispersive-x-ray fluorescence (EDXRF), Fourier transform infra-red (FTIR) spectroscopy, thermogravimetric differential thermal analysis (TG-DTA), nitrogen adsorption-desorption (Brunaue-Emmit-Teller (BET) and Barrot-Joyner-Halenda (BJH)) analysis to determine the crystallite size, band gap energy, elemental composition, functional group, thermal stability, specific surface area and pore size respectively. However in XRD analysis, the XRD patterns of as synthesized catalysts were recorded using Philip Pert powder x-ray diffractometer (Philip Pert-X ; Philip-Pert Company) having CuK_α radiation (λ= 1.56877Å, 30kVand 30mA) and scanned at the rate of 0.05s/step and 2θ range of 0 to 70°. For the band determination, Perkin Elmer diffuse reflectance ultra violet-visible spectrophotometer (Perkin Elmer Lambda-35; Elmer Company) was used to measure the band gap energy of the as synthesized catalysts. It is done by scanning of a catalyst over wavelength range of 200-800 nm. For the measurement of elemental composition an EDXRF Spectrometer (E-max-80; E-max company) was used, Similarly, for determination of functional group of developed ZnO NPs a FT-IR – Spectrophotometer (Agilant Carry-35; Agilant Company) was used. While thermal stability was determined using PerkinElmer thermal analyser (version-43; Toledo Company). Lastly the specific surface area and pore size distribution were estimated using Quantachrome (version-11.03) in which N_2 gas was used as adsorbate during the analysis.

2.6 Scanning and calibration experiments

To determine the maximum wavelength (λ_{max}) and calibration curve for the EBT and MB dyes, a stock solution (1000.00 mg/L) was prepared by dissolving 1000.00 mg (1.00 g) of the desired dye (EBT or MB) in 1000 cm^3 (1.00 L) of deionized water in a non-transparent amber bottle. Thereafter a series of the concentrations such as 2.00, 4.00, 6.00, 8.00, 10.00, 12.00 and 14.00 mg/L were prepared from the mother solution using dilution formula. However, deionized water was used to zero the Perkin-Elmer lambda 35 UV-Visible Spectrophotometer. The spectrum was taken in the range of 200 – 800 nm. The highest peak was for EBT and MB were taken and used during the entire experimental procedure. The calibration plot of absorbance versus concentrations was used to convert absorbance data into concentration via Beer Lambert law.

2.7 Photocatalytic experiment

In this work, the photocatalytic performance of the ZnO has been evaluated in the degradation of eriochrome black t and methylene blue dyes under ultraviolet (UV) light (96 W tungsten lamp) irradiation in a typical photoreactor. The amount of photocatalyst determined in the experiment plan was dispersed in 200 mL of dye solution (10 mg/L EBT/MB dye. Where required, the pH of the solution was adjusted using 0.05 M NaOH and 0.05 M HCl solution. During the reaction process, oxygen was continuously bubbled through the mixture to avoid change in the concentration of dissolved oxygen. Before light irradiation, the solution was stirred for 20 min in the dark at room temperature to reach the adsorption-desorption equilibrium.. Thereafter, aliquots of 5.00 ml test samples were let out of the sampling tab at periodic intervals of time (20 min), which was immediately filtered with cellulose nitrate filter (0.45 μm) to separate ZnO from the solution. The residual concentration of EBT and MB dyes solution were measured at 521 and 661 nm respectively using Perkin Elmer Lambda 35 UV-Vis spectrophotometer. The percentage efficiency (D %) was be calculated using Equation 1

$$D\% = 1 - \frac{[dye]_t}{[dye]_0} \times 100 \quad (1)$$

Where $[dye]_o$ and $[dye]_t$ are the initial and final concentration of dye, and t is the irradiation time. The effects of EBT and MB dyes initial concentrations, catalyst dosage, initial pH and initial temperatures were investigated and the degradation efficiencies were calculated using Equation 1.Similarly, a comparative study such as dark adsorption and photolysis over the biosynthesized ZnO NPs was also determine. These was compared with photocatalysis over ZnO photocatalyst.

2.8 Control experiment

Systematic control experiments for the photocatalytic degradation of EBT and MB over the ZnO catalyst under ultraviolet (UV) (96 W halogen lamp) irradiation and natural sunlight illumination at optimal reaction conditions were conducted and compared with the photocatalysis of EBT and MB using ZnO catalyst under visible (300 W Xenon lamp emitting at 400 nm) light irradiation.). The percentage removal were calculated using Equation 1

2.9 Radical scavenger tests

To investigate the major role of reactive radicals that was generated during the photocatalytic removal of EBT and MB over ZnO NPs, the main reactive radicals and holes was detected through radical scavenging experiments. During the photocatalytic process, the holes (h^+), hydroxyl radical (•OH) and superoxide radical ($•O^-_2$) are trapped by adding ammonium oxalate (AO), (h^+ scavenger), *t*-butanol ((•OH scavenger), and *p*-benzoquinone (($•O^-_2$ scavenger) into the reaction solution respectively. Typically, 10.00 mg of ZnO NPs and 10.00 mM of radical scavengers was introduced into 10.00 mg/L of EBT/MB solution, then the suspension was irradiated using the 96 W of tungsten lamp emitting at

253 nm for the same time. Finally the EBT/MB photodegradation efficiencies were calculated using Equation.

2.10 Durability tests

In order to evaluate the durability of the ZnO nanoparticles, a systematic experiment was performed at the optimum conditions of the photocatalytic removal of EBT and MB dyes over the ZnO NPs. Residual catalyst from degradation experiment was filtered, washed and dried and then recycled in fresh experiment and the percentage degradation was calculated using Equation 1

2.11 Kinetic profile

To investigate the kinetics of the photocatalytic degradation of EBT and MB dyes using biosynthesized ZnO NPs, experiments were conducted at optimal conditions and kinetic data were tested using the pseudo-zeroth order, pseudo-first order and pseudo-second order kinetic models as presented in Equation 2-4

$$\frac{[\mathrm{dye}]_0}{[\mathrm{dy}]_\mathrm{t}} = -k\ \mathrm{t} \tag{2}$$

$$\ln\frac{[\mathrm{dye}]_0}{[\mathrm{dy}]_\mathrm{t}} = k_{app}\ \mathrm{t} \tag{3}$$

$$\frac{1}{[\mathrm{dye}]_\mathrm{t}} - \frac{1}{[\mathrm{dye}]_0} = k\ \mathrm{t} \tag{4}$$

Where $[\mathrm{dye}]_0$ and $[dye]_t$ are the initial and final concentration of eriochrome black t/methylene blue, t is the irradiation time, k and k_{app} are the rate constant and apparent rate constant respectively for pseudo-zeroth, pseudo-second order and pseudo-first order reactions respectively. The basic kinetic parameter (*k)* was calculated from the plot of $\frac{[\mathrm{dye}]_0}{[\mathrm{dye}]_\mathrm{t}}$ against *t* for pseudo-zero order kinetics. Similarly, a plot of $\ln\frac{[\mathrm{dye}]_0}{[\mathrm{dye}]_\mathrm{t}}$ versus *t* gave a linear graph that passing through the origin and the apparent rate constant; k_{app} (min^{-1}) was estimated from the slope. While the plot of $\frac{1}{dye}$ against *t* also gave a linear graph that passing through the intercept in which the EBT/MB initial concentration was calculated from intersect and rate constant (*k*) from the slope.

2.12 Thermodynamic scheme

To determine the effects of crucial and important parameters such as activation energy ($\mathrm{E_a}$), enthalpy change (ΔH), entropy change (ΔS) and Gibbs free energy change (ΔG) for the photocatalytic removal of eriochrome black t and methylene blue over zinc oxide catalyst, an experiments were conducted at different temperatures (30, 40, 50, 70 and 90 ℃). At each temperature, the concentration of corresponding dye was determined at different interval of time (20.00 min) and the apparent rate constant (k_{app}) was determined using pseudo-first kinetic (Equation 3). Furthermore, at each 30, 40, 50, 70 and 90 ℃ the corresponding k_{app} were calculated and the activation energy for the processes was determine using Svent Arrhenius expression (Equation 5)

$$\ln k_{app} = \mathrm{In\ A}\ - \frac{\mathrm{E_a}}{\mathrm{R}}\left(\frac{1}{\mathrm{T}}\right) \tag{5}$$

Where k_{app} is apparent rate or velocity constant, A is the pre-exponential or stearic factor, E_a is the activation energy, R is the molar gas constant and T is the temperature. The plot of $ln\ k_{app}$ versus $\frac{1}{T}$ yield a linear graph with the intercept in which theE_a can be obtained from the slope and A from the intercept While ΔH, ΔS and ΔG for the photocatalytic removal of EBT and MB dyes were obtained using the following expressions (Equation 6-8)

$$\Delta\mathrm{H} = \mathrm{E_a} - \mathrm{RT} \tag{6}$$

$$\ln\left(\frac{k_{app}}{\mathrm{T}}\right) = -\frac{\Delta\mathrm{H}}{\mathrm{R}}\left(\frac{1}{\mathrm{T}}\right) + \frac{\Delta\mathrm{S}}{\mathrm{R}} + \ln\left(\frac{\mathrm{k_B}}{\mathrm{h}}\right) \tag{7}$$

and

$$\Delta\mathrm{G} = \Delta\mathrm{H} - \mathrm{T}\Delta\mathrm{S} \tag{8}$$

Where k_B is Boltzmann constant, h is planck's constant, ΔS is entropy change and ΔG is the Gibbs free energy change. Similarly, Plotting $\ln\left(\frac{k_{app}}{\mathrm{T}}\right)$ against $\frac{1}{T}$ gave a linear graph with intercept in which ΔH was evaluated from the slope and ΔS was calculated from the intercept. While equation 4 and 6 were used to determine the enthalpy change and Gibbs free energy change at various temperatures.

3. RESULTS AND DİSCUSSİON

3.1 Characterization of ZnO NPs

3.1.1 Thermogravimetric differential thermal analysis (TG-DTA)

In order to estimate the thermal stability and thermodynamic parameters such as thermal activation energy, enthalpy, entropy and Gibbs free energy of activation [49-51] of decomposition processes for the biosynthesized ZnO NPs, a thermogravimetric differential thermal analysis (TG-DTA) was performed and the result obtained is presented in Figure 2. TG measurement is primarily used to estimate the composition of ZnO photocatalyst and to predict their thermal stability up to

elevated temperatures while DTA is primarily used to determine the exothermic and endothermic nature of the processes [49]. However, the TG-DTA of the studied catalysts was conducted from 30-950 ℃ at heat rate 10.00℃/min as typical calcination temperature for ZnO and fall between 500.00-888.40 ℃. However, it can be seen that Figure 2 shows that there was consecutive weight loss in ZnO catalyst precursors at different stages. It is also clear from Figure 2 that there were three steps of decomposition processes during the biosynthesis of ZnO NPs. Furthermore, Table 1 represents the decomposition steps, temperature, and peak temperature and weight loss for ZnO photocatalyst. The result presented in Table 1 indicates that in the first decomposition step, there is a minor percentage weight loss (4.12 %) at around 34.00-320.00 ℃ due to moisture and volatile solvent desorption for the ZnO [51, 52]. The second decomposition step is the major percentage weight loss (84.98 %) in the temperature range of 320.00-530.00 ℃ is due to the adsorbed gases such as carbon (iv) oxide (CO_2), carbon (ii) oxide (CO) and intrinsic water crystallization (H_2O) in the decomposition [53]. The latter process in the TG-DTA thermogram there is insignificant percentage weight loss of H_2O and CO_2 (3.00 %) in the temperature range 530.00-870.00 ℃ for the ZnO NPs. This shows that the decomposition of catalyst precursor is almost completed before 600.00 ℃ was attained. This implies that 600.00 ℃ would be a satisfactory temperature for the precursor decomposition. The chosen temperature for calcination of ZnO catalyst precursor was 600.00 ℃ as the final percentage weight loss even begins before this point for the ZnO photocatalyst.

The difference in thermal decomposition behaviour of the studied photocatalyst can be seen more clearly from curves shown in Figure.2. TG-DTA curves show three temperature broad peaks T_k corresponding to three decomposition region (Table 1) for the ZnO NPs. It is noted that the peak temperature T_k of TG-DTA of ZnO in all regions are shifted to lower temperatures.
According to the Coats-Redfern method for first order reaction (Equation 9),

$$\ln\left[\frac{-\ln(1-\delta)}{T^2}\right] = -\frac{E^*}{RT} + \ln\frac{AR}{\beta E^*} \quad (9)$$

Where A is constant, β is the heating rate, R is the universal gas constant, δ is fraction of decomposition and E^* is the activation energy. Therefore the plotting $\ln\left[\frac{-\ln(1-\delta)}{T^2}\right]$ against 1/T according to the equation 7 should give a straight line whose slope is directly proportional to the activation energy ($-\frac{E^*}{RT}$).

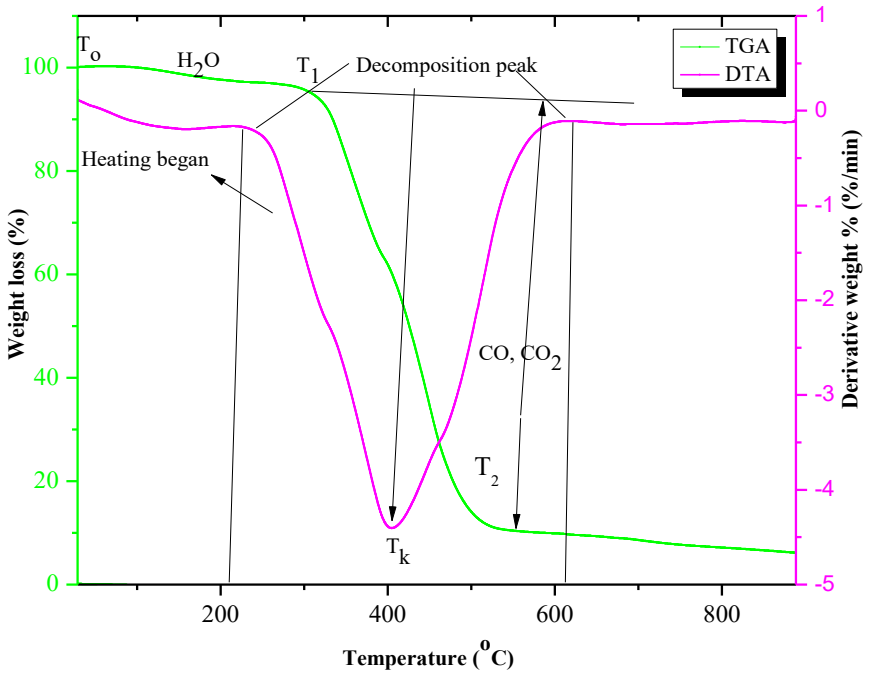

Figure 2 TG-DTA curve of ZnO nanoparticles

Table 1: TG-DTA data for the biosynthesized ZnO photocatalyst

Catalyst	Region of decomposition	Temperature (℃) Start	End	Peak Temp	Weight loss (%) Partial	Total	Residual	Comments
	1st	34	320	100	4.12			Loss of water
ZnO	2nd	320	530	230	84.98	92.00	8.00	Loss of CO_2
	3rd	530	870	410	88.00			All most complete

T_p : Peak temperature of TG-DTA

The activation entropy,ΔS^*, the activation enthalpy ΔH^*, and the free energy (Gibbs function ΔG^*) were calculating using the following expression (Equation 10-12) [51]

$$\Delta S^* = 2.303 \left[\log \frac{Ah}{kT}\right] R \quad (10)$$

$$\Delta H^* = E^* - RT \quad (11)$$

$$\Delta G^* = \Delta H^* - T\Delta S^* \quad (12)$$

However, the calculated thermodynamic parameters values are given in Table 2.

Table 2: TGA-DTA thermodynamic parameters for ZnO photocatalyst

Catalyst	E^* (kJ mol^{-1})		ΔS^* (JK^{-1} mol^{-1})		ΔH^* (kJ mol^{-1})		ΔG^* (kJ mol^{-1})	
	2nd	3rd	2nd	3rd	2nd	3rd	2nd	3rd
ZnO	+123	+165	-45	-35	+130	+ 120	+146	+ 178

From the result presented in Table 2, it is clear that the values of ΔH^*, ΔG^* and ΔS^* for the biosynthesized catalyst increases from the second to third decomposition steps. This indicates that moving from one decomposition step to another cause an increase of thermal motion and a decrease of both thermal stability and the ordered of that system. Comparing these results, the nature of the second decomposition region is relatively low thermal motion, more orderliness and relative thermal stability of most samples with respect to the third decomposition process. The activation energies for this system are small at second stages of decomposition and high at the high stages. These lower values are most likely associated with the processes that occur during the formation of Zn-O system [53]). Additionally, the positive value of ΔG^* and negative value of ΔS in the second and third steps for the decomposition processes indicated that the process is non-spontaneous while the positive signs for the ΔH^* shows that the decomposition process during the biosynthesis of ZnO NPs is endothermic in nature.

3.1.2 X-ray diffraction (XRD) analysis

In order to determine the microstructure, lattice phase, average crystallite size, lattice strain, specific surface area, morphology index and purity for the biosynthesized ZnO NPs, an x-ray diffraction (XRD) analysis was conducted and the result obtained is displayed in Figure 3.

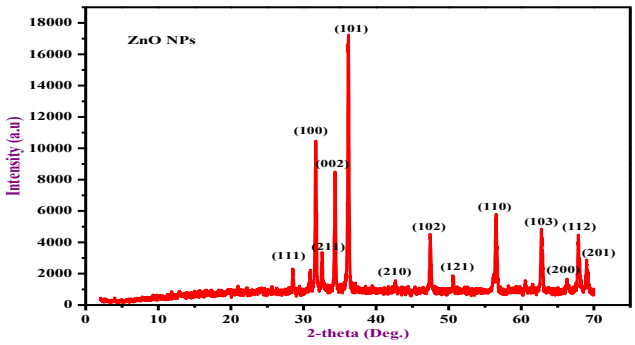

Figure 3 XRD patterns of biosynthesized ZnO NPs

As observed in Figure 3 the intense peaks at 2θ values of 28.52, 30.90, 31.68, 32.53, 34.34, 36.17, 42.56, 47.44, 50.65, 56.12, 56.50, 60.59, 62.76, 66.31, 67.85 and 68.99° were corresponds to the miller index plane (111), (100), (002), (211), (101), (210), (102), (121),(110), (103), (200), (112) and (201) of ZnO NPs respectively. These patterns of the bioprepared ZnO nanoparticles were consistent with that of the standard wurtzite structure of ZnO (JCPDS card no. 04-005-4711).

Furthermore, there were no impurity peaks in the observed XRD pattern indicating that the biosynthesized photocatalysts were pure. To confirm the crystal structure and shape, the structural parameters like interspacing distance, lattice parameters -such as a, b, c and volume of unite cell of the prepared catalyst was calculated and compared with that of standard (Equation 13-15) [50]

$$a = b = \frac{\lambda}{\sqrt{\sin\theta_{100}}} \quad (13)$$

$$c = \frac{\lambda}{\sin\theta_{002}} \quad (14)$$

$$V = 0.866 \times a^2 \times c \quad (15)$$

The plane d-spacing (d_{hkl}) with the lattice parameters a, b and c and the Miller indices (hkl) is calculated via the theoretical Equation 16 and Bragg Equation 17

$$\frac{1}{a^2} = \left[\frac{h^2+hk+k^2}{a^2}\right] + \frac{l^2}{c^2} \quad (16)$$

$$d = \frac{\lambda}{2\sin\theta_{100}} \quad (17)$$

Where a, b and c are the lattice constants, λ is the wavelength of X-ray radiation (1.5406 Å), θ is the Bragg angle, d_{hkl} is the spacing distance, hkl is the miller indices, and V is the volume of unit cell. The calculated a, b and c values for the prepared ZnO NPs are presented in Table 3.

Table 3: Structural parameters of ZnO photocatalyst

Catalyst	d_{100} (Å)	Lattice parameter (Å)		Crystal structure	c/a	Volume of unit cell (Å)
		a = b	c			
ZnO	2.8115	3.2466	5.2031	Hexagonal wurtzite	1.6026	47.4939

Note that: the ratio c/a is the relationship between the lattice parameter of he synthesized ZnO NPs

From the Table 3, the estimated structural parameters values for bio-prepared ZnO NPs were matched with that of standard hexagonal wurtzite structure of ZnO[54]. These also clearly indicated that the bio-prepared ZnO was the hexagonal wurtzite in nature. While the average crystalline size of the as biosynthesized catalysts was obtained by using a well-known expression of Debye-Scherer equation (Equation 18) [54]

$$D = \frac{k\lambda}{\beta\cos\theta} \quad (18)$$

where D is the average particle size, k is the Debye- Scherer (D-S) constants 0.89, λ is the wavelength of the x-ray radiation, β is the full width of half maximum intensity (FWHM) in radiation, θ is the diffraction angle at the position of peak maximum. The relationship between the crystallite size and lattice strain due to crystal imperfection and distortion was studied using the Williamson-.Hall method (Equation 19). [55, 56],

$$\beta\cos\theta = \frac{k\lambda}{D} + 4\varepsilon \times \sin\theta \quad (19)$$

where D and ε are the crystallize size and lattice strain respectively. The crystallite size was calculated from y intersect of the plot βcosθ against sinθ. While the lattice strain (ε) was calculated from the slope. However, the XRD row data also were used to estimate the SSA of the as synthesized ZnO, via the following theoretical equation (Equation 20 and 21),

$$SSA = \frac{6000}{D\times\rho} \quad (21)$$

$$SSA = \frac{S.A}{V \times \rho} \quad (20)$$

where V is the volume of unit cell, SA is the surface area, ρ is the density of catalyst and SSA is the specific surface area. While the bond length for the bio-prepared Zn-O bond was calculated using Equation 22 [57],

$$L = \sqrt{\left[\left(\frac{a^2}{3}\right) + (0.5-\mu)^2 \times c^2\right]} \quad (22)$$

where L is the bond length, (μ) is the positional parameter of the wurtzite structure that indicates the extent of atoms displacement relative to the following plane in c axis as expressed with equation (Equation 23) [58].

$$\mu = \frac{a^2}{3c^2} + 0.25 \quad (23)$$

Moreover, the average crystallite size, surface area, lattice strain and bond length were also estimated for ZnO catalyst and the results are presented in Table 4.

Table 4: Average crystallite size of ZnO NPs estimated using Debye-Scherer and Williamson-Hull equation.

Catalyst	Crystallite size, D-S (nm)	Crystallite size, W-H (nm)	Lattice strain (Ɛ x 10^{-3})	Surface area (m^2g^{-1})	Bond length L (Å)
ZnO	50.10	87.23	3.11	74.98	1.951

The results in the Table 4 elaborates that the average crystallite size of the ZnO) was found to be 50.10 nm (Table 4). On the other hand the surface of ZnO was found to be 74.98 m^2g^{-1}. These indicate that as the average crystallite size decreases and the surface area of ZnO was increased [57]. These finding were in good agreement with many results reported in the literature 41, 42,[44, 45, 57, 58]. However, the surface area for ZnO catalyst was estimated by the Debye-Scherer's (D-S) and Willianmson-Hull (W-H) models and the results were compared in which the surface area estimated by W-H model is higher than the one estimated by the D-S. These differences might to arise due the different models but the two models followed the same

trend. On the other hand the estimated bond length value of ZnO was found to be 1.951 Å (Table 4).

3.1.3 FT-IR analysis

The functional groups and vibration bond of the bio-synthesized photocatalyst was determined by the FT-IR spectrum in the wavenumber range 4000-500cm^{-1}[58, 59]. The FT-IR spectrum of the ZnO catalyst is depicted in Figure 4.

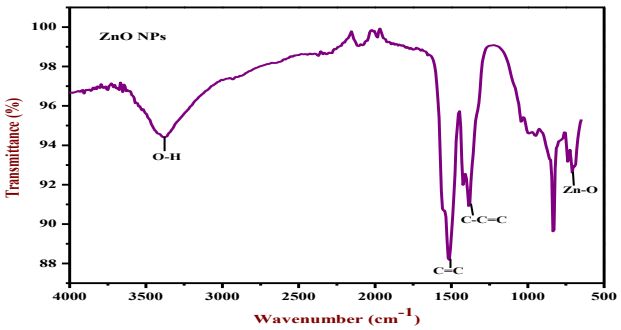

Figure 4. FT-IR spectrum of ZnO NPs

Figure 4 indicates the present of different functional groups and their corresponding vibration bonds and the summary is presented in Table 5.

Table 5: Functional groups and the vibration bonds present in the, ZnO nanoparticles

S/NO	Catalyst	Wavenumber (cm^{-1})	Functional Group
1	ZnO	3315	O-H stretching vibration
		1447	C-C=C vibration bonds
		1665	C=C vibration bond
		637	Zn-O stretching vibration

However, the result presented in Table 5 demonstrates that the peaks appear at 3315 cm^{-1} corresponding to the vibration bonds of O-H from suspension of hydroxyl group in adsorbed water [58]). The peaks observed at 1447, and 1665 cm^{-1} corresponding to the vibration bonds of C=C-C and C=C tensile vibration respectively [59-61]. While the peaks at 637 cm^{-1} ascribed to the stretching vibration bond of Zn-O [62]. The bonding could occur through the sharing or transfer of electrons between these elements. The Zn-O bond might suggest that the Zn and O has been chemically reacted.

3.1.4 EDXRF analysis

To determine the elemental composition present in the biosynthesized ZnO catalyst is of great importance. Energy Dispersive X-ray Fluorescence (EDXRF) analysis was conducted and the result obtained for ZnO is presented in Figure 5. As seen in Figure 5, the present of the prominent peaks at 8.40 and 8.60 KeV which correspond to the zinc (Zn) atoms with no other undefined and insignificant peaks. This confirmed that the sample was pure ZnO nanoparticles Therefore, present of Zn atom, clearly confirmed the EDXRF spectrum of ZnO NPs. However, these results were in good agreement with the results obtained from the FT-IR analysis. Furthermore, the constituent elements and it percentage composition present in ZnO photocatalyst is presented in Table 6.

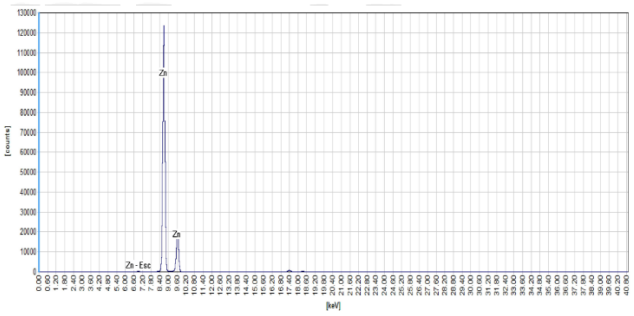

Figure 5. EDXRF spectrum of ZnO NPs

Table 6: EDXRF elemental composition of ZnO photocatalyst

Element	Composition (%)
Fe	0.0127
Co	0.2482
Ni	0.0149
Zn	55.602
Ga	0.0274
Ta	0.3490
C	1.8680
Au	0.1126
Al	0.1040
Si	0.0707
S	0.6315
Cl	0.0143
K	0.0023
Ti	0.0135
Mn	0.0001
As	0.0006
Rb	0.0000053
Y	0.000996
Zr	-0.02000
Nb	0.0784
Mo	-0.000
Bi	0.03911
Pb	0.0002
Th	0.00065
Ag	0.00054
Ce	0.0083
Total (%)	**96.422**

Where total percentage composition of elements detected in ZnO = 59.180 %, Zn = 55.602 %, O = 40.820 % and trace elements (impurities) = 3.578 %. According to the Table 6,

the percentage composition of ZnO was found to be 96.422 % in which Zn = 55.602 %, O = 40.820 % and trace elements = 3.578 %. These indicated that the biosynthesized ZnO is pure. Moreover, these results were supported the FT-IR and XRD analyses and many other previous related works in the literature [63, 64].

3.1.5 UV/Vis analysis

Band gap energy (E_g) is a one of the important parameter that determined the photocatalytic performance of a good catalyst. In this paper, Perkin Elmer diffuse reflectance ultra violet-visible spectrophotometer was used to measure the band gap energy of the as biosynthesized ZnO catalyst. It is done by scanning of a catalyst over wavelength range of 200-800 nm. The band gap (E_g) for the ZnO NPs was calculated from electronic data recorded by the UV/Visible spectrophometer using Schuster-Kubelka-Munk relations (M-K) (Equation 24).

$$(\alpha h\nu)^{\frac{1}{n}} = K(h\nu - E_g) \quad (24)$$

where α is the absorption coefficient obtained from Beer's – Lambert law, h is the planck's constant, ν is the frequency of vibration, K is the proportionality constant and E_g is the band gap energy of the semiconducting material. The E_g value was calculated from intersect of the plot $(\alpha h\nu)^{\frac{1}{n}}$ against hν and the K was obtained from the slope. The result obtained for this analysis was displayed in Figure 6.

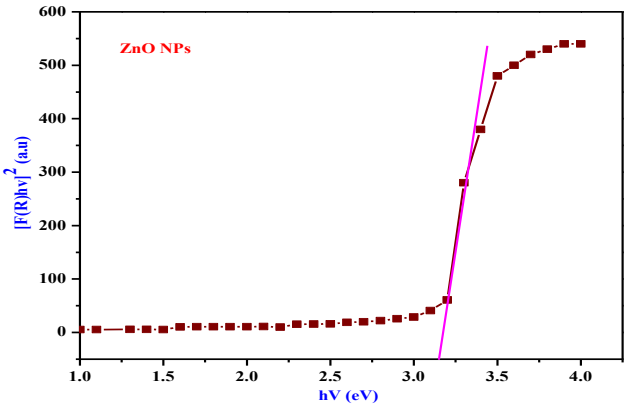

Figure 6. Tauc 's plot of ZnO

Figure 6 shows linearity in the vicinity of the band gap region for the ZnO photocatalyst revealing that the ZnO crystal structure did not change the direct electron transition characteristics of the ZnO [65]. The band gap energy value for the ZnO catalyst was found to be 3.25 eV. The value obtained (3.25 eV) was consistent with bandgap of conventional ZnO NPs recorded in the recent previous related works [39, 40, 41, 42, 44]. This confirming the ability of the synthesized ZnO to relatively absorb more UV light. As a result, the ZnO nanoparticle is an excellent conductor and can be used as an electrophotocatalyst in the photoelectrochemical reactions [66].

3.1.6 BET analysis

Surface area is a one of the crucial factor that plays an important role in determining the catalystic activities of a catalyst because it provides more active sites on the surface of good catalysts [67]. The surface area, pore size and pore volume of the ZnO were determined by N_2 adsorption-desorption isotherms and their results are shown in

7.

Table 7 Surface area, pore volume and pore size of ZnO photocatalyst

Catalyst	Model	Surface area (m^2g^{-1})	Pore volume (ccg^{-1})	Pore size (nm)
	Single point BET	101.01	-	-
	Multipoint BET	190.04	-	-
	Langmuir	4652.82	-	-
	BJH	190.303	92.6200	3.28
ZnO	DH	202.01	946.70	2.14
	t-method	190.00	-	-
	DR	188.20	668.80	6.52
	DFT	39.64	480.40	2.65
	HK	-	262.00	1.85
	SF	-	430.10	3.50
	DA	-	-	3.00

From the result presented in Table 7, the surface area, pore size and pore volume were determined by the different models. But the multipoint Brunauer-Emmiitt-Teller (BET) and Barrett-Joyner-Halender (BJH) are the most promising, widely and acceptable models used for determining the surface area, pore size and pore volume of a catalyst in many literatures [68]. Because of the above mentioned reasons, the summary of the multipoint BET surface, BJH pore size and BJH pore volume for the ZnO, is shown in Table 8.

Table 8 Multipoint BET surface, BJH pore size and pore volume of ZnO photocatalyst

Catalyst	BET surface area (m^2g^{-1})	BJH pore size (nm)	BJH pore volume (ccg^{-1})
ZnO	190.04	3.275	5.96×10^2

The result presented in Table 8, the multipoint BET surface area (S_{BET}) was found to be 190.04, m^2g^{-1} for ZnO catalyst. As observed in the Table 8, the higher the surface area, the lower the lower the pore size and pore volume of a catalyst and vice versa. These finding were in good agreement with many results presented in previous related works [68, 69]. Additionally the particle distribution and N_2 adsorption-desorption isotherm for the bio-prepared ZnO catalysts are depicted in Figure 7. As seen from the Figure 7 (a) the pore size for the prepared catalyst is within the porosity range from 2.00-50.00 nm. Therefore, it can be concluded that the biosynthesized ZnO photocatalyst is mesoporous or mesopore in nature. While Figure 7 (a1) revealed that the data obey the adsorption isotherm type-IV for the hysteresis loops. However, these findings were in good agreement with many previous recent related works in the literatures [68].

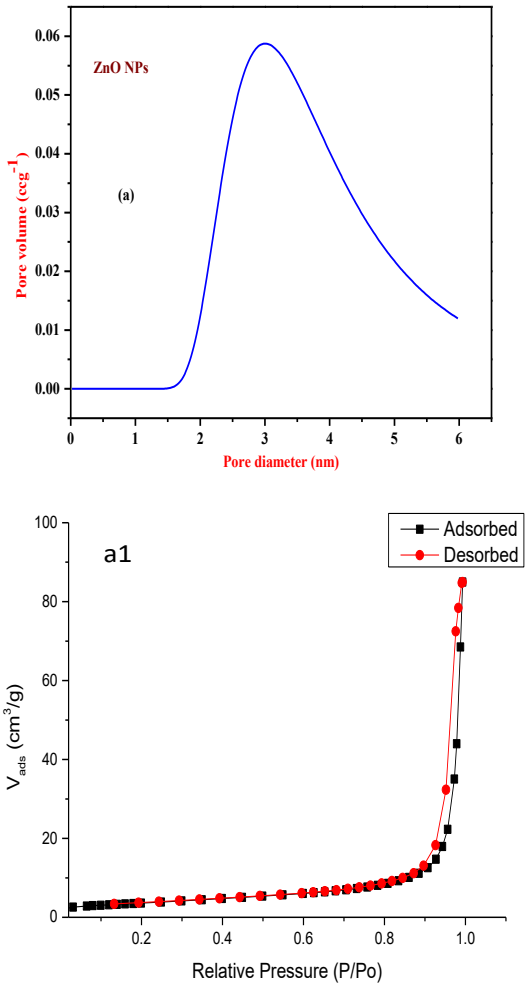

Figure 7 (a) Particle distribution (a1) N_2-adsorption-desorption isotherm of bio-prepared ZnO photocatalyst

3.2 Evaluation of the photocatalytic activity of bio-prepared ZnO NPs

3.2.1 Scanning and calibration curve of EBT and MB dyes

To determine the maximum wavelength (λ_{max}) and calibration curve for the eriochrome blact t and methylene blue dyes, stock solution of for each EBT and MB was prepared by dissolving 100 mg (0.1 g) of dye with 1 liter of deionized water in a non-transparent container (Amber bottle). Then 2, 4, 6, 8, 10, 12 and 14 mg/L of EBT/MB solutions were prepared from stock solution using dilution formula. A blank sample of deionized water was used to zero the Perkin-Elmer lambda 65 UV-Visible Spectrophotometer. The spectrum was taken in the range of 200 – 800 nm. The highest peak for EBT/MB was taken and used during the entire experimental procedure. The calibration plot of EBT/MB dye of absorbance vs concentration was used to convert absorbance data into concentration of EBT/MB solution using the Beer Lambert law.

The result for the scanning of EBT dye is depicted in Figure 8 (a). It can be seen from the Figure 8 (a) that the λ_{max} of EBT was found to be 521 nm which was used throughout the photocatalytic experiments in this work. The calibration curve for the EBT with correlation coefficient (R^2) of 0.9956 is illustrated in Figure 8 (b). While result obtained for the scanning of MB dye is presented in Figure 9 (a). It can be seen from the Figure 9 (a) that the λ_{max} for MB was found to be 668 nm which was used throughout the photocatalytic experiments. The calibration curve for the MB dye with correlation coefficient (R^2) of 0.9971 is display in Figure 9 (b).

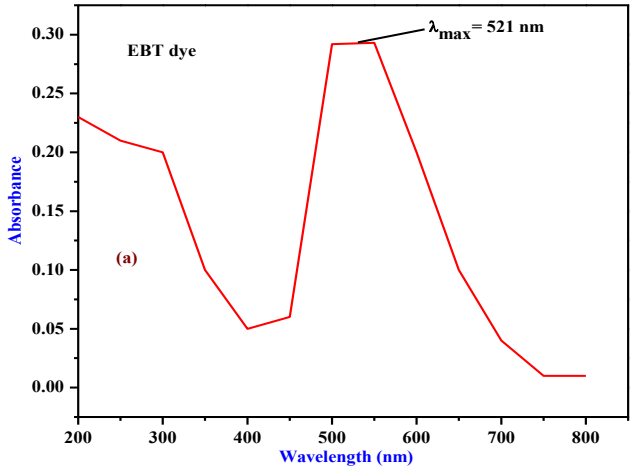

Figure 8 (a) Scanning of EBT dye to determine the maximum wavelength

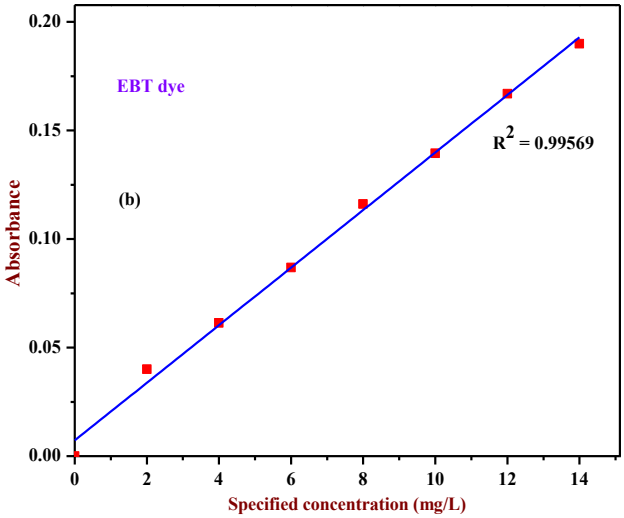

Figure 8 (b) Calibration Curve of EBT dye at λ_{max} = 521 nm

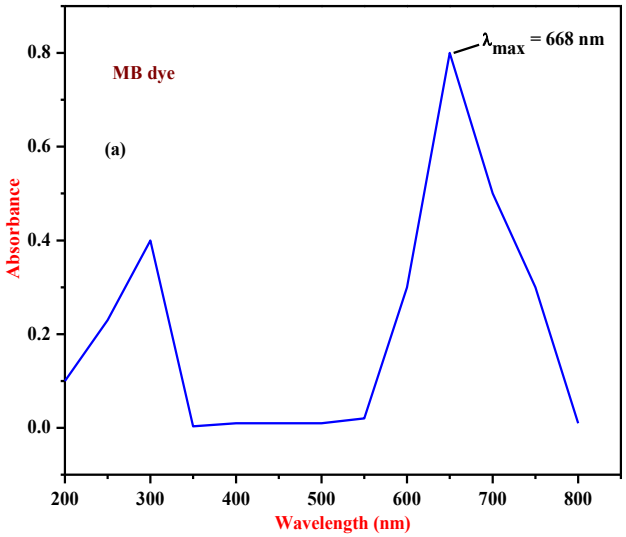

Figure 9 (a) Scanning of EBT dye to determine the maximum wavelength

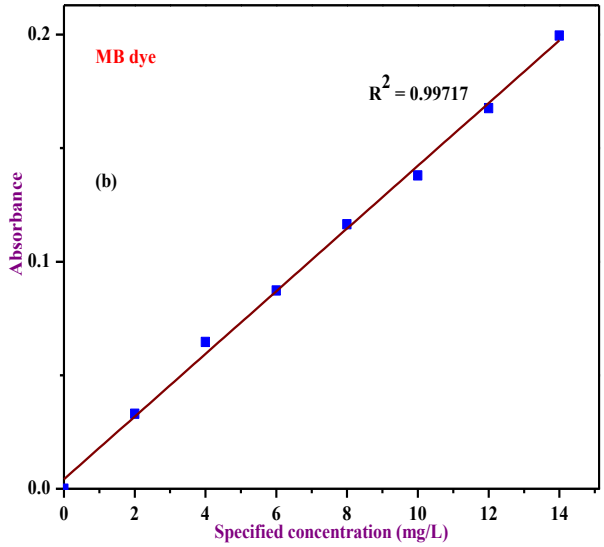

Figure 9 (b) Calibration Curve of EBT dye at λ_{max} = 668 nm

3.2.2 Effect of initial concentrations

To determine the effect of initial concentrations for the EBT and MB dyes, experiments were conducted by varying the initial concentrations of EBT /MB (10-50 mg/L). The amount of the ZnO (1.5 g/L), initial pH (9) of the suspension, volume of the solution (200 mL), irradiation time (120 min) and temperature (50 ℃) were kept constant and the results obtained is presented in Figure 10. It can be seen from the Figure 10 that the percentage degradation efficiency increases with decreasing of the EBT and MB initial concentration. For instance the optimum degradation efficiencies (98.05 and 97.51 %) were obtained at 10 mg/L

initial concentration of EBT and MB dyes respectively in 120 min irradiation time. This is because the number of photons absorption by the catalyst increases in the lower concentration regime. This suggests that as the initial concentration of EBT increases the requirement of the photocatalyst surface needed for the degradation also increases. Since the irradiation time and amount of the ZnO NPs are constant, the •OH radical (primary oxidant) formed on the surface of ZnO is also constant. Furthermore, the relative number of the free radical attacking the EBT/MB molecule decreases with increasing amount of the photocatalyst [70]. While the percentage photo removal of EBT/MB decreases with the increasing of the EBT/MB initial concentration. This is because the number of photons absorption by the ZnO photocatalyst decreases in the higher concentration of EBT/MB and requirement of the ZnO surface required for the degradation also increases. These findings were consistent with the work reported by Abdu *et al* [71] and Kansal *et al* [72].

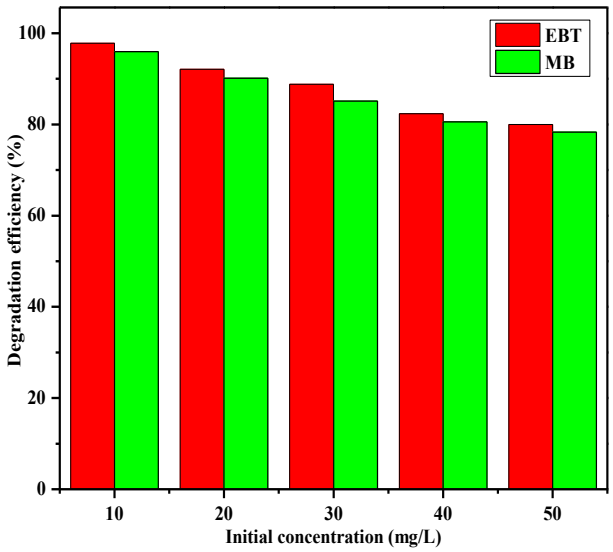

Figure 10. Effect of initial concentration on the photocatalytic removal of EBT and MB dyes over ZnO nanoparticles

3.2.3 Effect of ZnO loading

To determine the optimum amount of ZnO loading in the photocatalytic removal of EBT/MB, various amount of ZnO (0.1-0.6 g/L) were used while the EBT/MB initial concentration, initial pH, volume of solution, temperature and irradiation time were kept constant. Figure 11 shows the effect of catalyst loading for the photocatalytic degradation of EBT/MB over the ZnO NPs. From the Figure 11, it can be seen that the increase in the amount ZnO from 0.5 to 3g /L slightly increases the percentage degradation of EBT/MB due to availability of active sites with increases of catalyst loading. Furthermore, decrease in the removal efficiencies of EBT/MB was observed at amount of ZnO above 1.5 g/L. Thus 1.5 g/L ((96.58 and 95.65 %) of ZnO photocatalyst was found to be the optimal amount when compared with the rest amount of catalyst in 120 min. The slight decrease in degradation of EBT/MB may be due to the aggregation of ZnO NPs. These findings were in good agreement with the previous related works [39, 66]

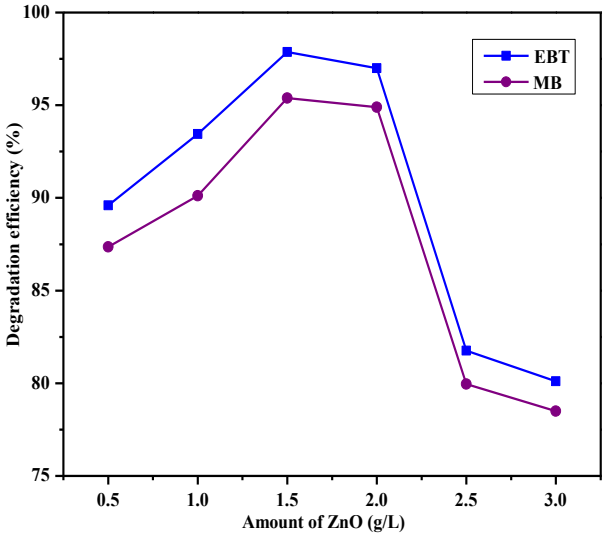

Figure 11. Effect of the amount of catalyst on the photocatalytic degradation of EBT and MB dyes over ZnO nanoparticles

3.2.4 Effect of initial pH

To determine the effect of initial pH on the photocatalytic removal of EBT and MB using ZnO photocatalyst, experiments were performed by varying the initial pH in the range (3-13). In the experiments pH was adjusted by adding appropriate drop of 0.05 M HCl or 0.05 M NaOH solution while the initial concentration, catalyst dosage, volume of solution, temperature and irradiation time were kept constant and the result is presented in Figure 12. From the Figure 12, it can be seen that there was a significant increase in the removal of EBT with an increase in initial pH. It is also observed that the percentage degradation of EBT is slightly increasing from 3-9 and decreases at the pH greater than 10. This clearly indicated that the optimum degradation efficiencies (96.45 and 94.98 %) for the photocatalytic removal of EBT and MB dyes over the obtained ZnO NPs were archived at initial pH of 9 in 120 min. This is because the solution pH affects the surface charge of ZnO and availability of hydroxyl radicals. At high pH values (greater than 9) the hydroxyl radicals are so rapidly scavenged that they do not have the opportunity to react with EBT/MB. The pH affects not only the surface properties of ZnO, but also the dissociation of EBT/MB and formation of hydroxyl radicals. Thus, the degradation of EBT/MB in this work was more efficient under basic (9) conditions than under acidic conditions. This is because under basic conditions, the •OH radicals are generated more easily by oxidizing more hydroxide ions available the catalyst surface and thus the efficiency of the process is enhanced. Similarly, at low pH, reduction by electrons in the conducting band may play a

very important role in the degradation of EBT/MB due to the reductive cleavage of azo bonds. These findings were consistent with previous studies [39, 66, 67]

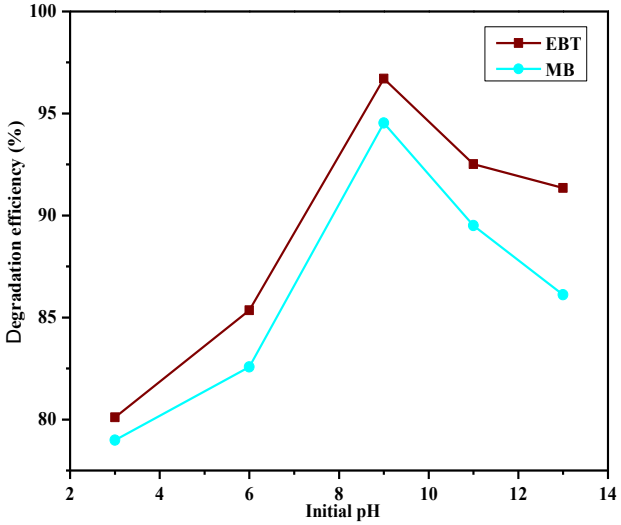

Figure 12. Effect of initial pH on the photocatalytic degradation of EBT and MB over ZnO NPs

3.2.5 Effect of temperature

To investigate the effect of temperature, experiments were conducted by varying the temperature 30.00, 40.00, 50.00, 70.00 and 90.00 ℃. While the amount of the ZnO, initial pH of the suspension, volume of the solution, irradiation time and EBT/MB initial concentration were kept constant and the results obtained is depicted in Figure 13. However, the result presented in Figure 13 demonstrated that the EBT/MB photoremoval efficiency increased progressively as the temperature increases roughly from 30.00-50.00 ℃. This indicated that the optimum photocatalytic degradation efficiencies (96.75 and 93.25 %) of EBT and MB over the ZnO nanoparticles were obtained at a temperature of 50.00 ℃ in 120.00 min. This might to be attributed to the fact that as the temperature increases from 30.00-50.00 ℃ the adsorption of the EBT/MB onto the surface of the ZnO catalyst and kinetic energy also increases and thus leads to the better degradation efficiency. These findings were in line with the previous works reported by Barakat *et al* [68] and Chen *et al* [69]. On the other hand the photocatalytic degradation of EBT/MB over ZnO catalyst decreased when the temperature is above 50.00 ℃. This shows that the adsorption capacity for ZnO catalyst declined as the higher temperature above the optimum levels. Similarly, as the temperature is higher than 50.00 ℃, the recombination of charge carriers will increase and active site of the ZnO catalyst will be decrease, become disfavored and subsequently lead to the decreased in the photocatalytic removal of EBT/MB. Moreover, these results were in good agreement with the study recorded by Parra *et al* [73] and Kumar *et al* [74].

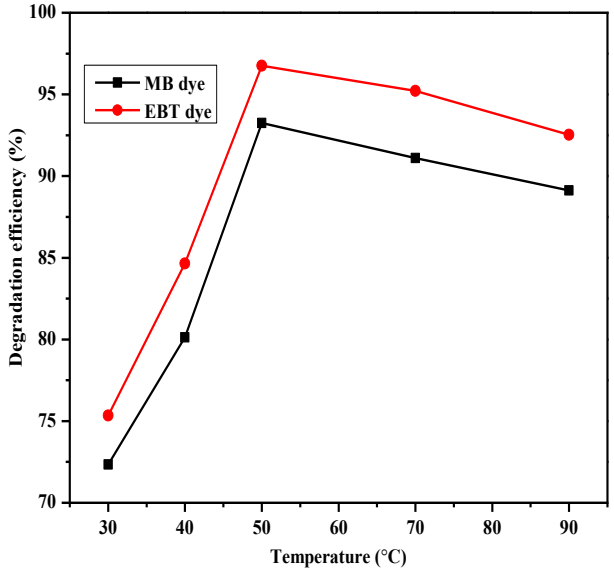

Figure 13. Effect of temperature on the photocatalytic degradation of EBT and MB dye over ZnO NPs

3.2.6 Control

To evaluate the photocatalytic degradation of EBT and MB dyes over ZnO photocatalyst, control experiments were performed under different experimental conditions (a) EBT photocatalysis (b) MB photocatalysis (c) adsorption and (d) photolysis. While the other conditions such as EBT/MB initial concentration, amount of ZnO catalyst, volume of solution, temperature, irradiation time and initial pH were kept constant and the result is displayed in Figure 14.

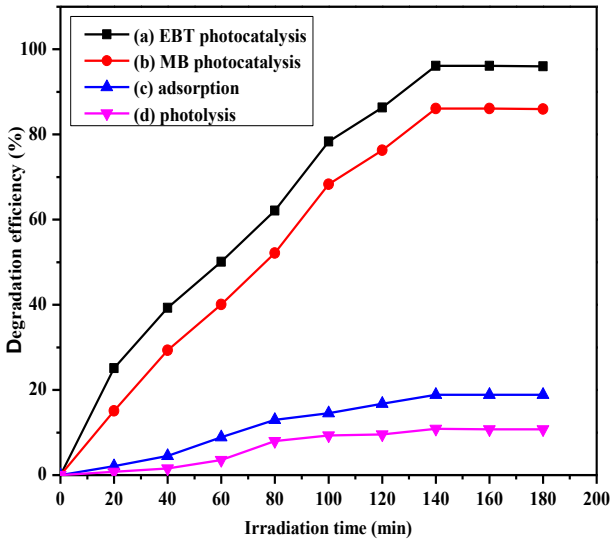

Figure 14. Control experiment (a) EBT photocatalysis (b) MB photocatalysis (c) adsorption (d) photolysis

According to the results presented in Figure 14, the photolysis (10.89 %) yields the insignificant responses

during the process while the adsorption (18.89 %) revealed the moderate and intermediate response. While the photocatalysis resulted the better and significant responses for the photocatalytic removal of EBT (96.11 %) and MB (86.12 %) using ZnO photocatalyst under UV light irradiation. These clearly demonstrated the light and photocatalyst were the two most significant and important factors that influencing the photocatalytic removal of EBT over the biosynthesized ZnO nanoparticles. These findings were also found to be in line with the previous related work investigated by Yusha'u *et al* [39].

3.2.7 Radical scavengers test and proposed mechanism

To investigate the roles and contributions of the hydroxyl radical (•OH), superoxide (O_2^-) and hole (h^+) generated during the photocatalytic degradation of EBT and MB over the ZnO photocatalyst. However, the main reactive radicals and holes were detected through radical scavenging experiments. During the photocatalytic process, the holes (h^+), hydroxyl radical (•OH) and superoxide radical ($•O^-_2$) are trapped by adding ammonium oxalate (AO), (h^+ scavenger), *t*-butanol (•OH scavenger), and *p*-benzoquinone ($•O^-_2$ scavenger) into the reaction solution respectively. While the other conditions such as EBT/MB initial concentration, amount of ZnO catalyst, volume of solution, temperature, irradiation time and initial pH were kept constant and the result is presented in Figure 15. Based on the results presented in the Figure 15, the holes, superoxide and hydroxyl radicals contributed immensely during the photocatalytic process as compared with the photocatalytic removal in the absence of scavengers. Moreover, among the most reactive radicals and holes, the hydroxyl radical showed the most significant responses on the photocatalytic removal of EBT and MB dyes using the ZnO photocatalyst under UV light irradiation as proved by given low yielded for the photocatalytic processes. Based on this result the •OH is key and important radical that leads the photoremoval of EBT and MB dyes over the developed catalyst. These findings were in line with the previous study reported by Yusha'u *et al* [9].).

A mechanism for photocatalytic removal of eriochrome black t/methylene blue dyes onto the surface of ZnO nanoparticle under UV irradiation is illustrated in Figure 16. According to the Figure 16, the electrons in valence band (VB) transfer to the conduction band (CB) under UV irradiation of the photocatalyst. The corresponding energy is higher than the band gap of the ZnO (3.18 eV) there by promoting the generation of conduction band electrons and valence band holes. The photogenerated holes (h^+) could either directly oxidize adsorbed EBT/MB or react with hydroxyl or hydrogen peroxide to generate hydroxyl radical. Similarly, the photoelectrons (e^-) reduce oxygen adsorbed on the photocatalyst surface into superoxide radical. Thereafter, the EBT/MB dye was degraded by generated hydroxyl and superoxide radical into environmentally friendly species carbon dioxide, water and byproduct according to the expressions (Equations 25-28).

$$TiO_2 + h\vartheta \rightarrow h^+ + e^- \quad (25)$$

$$h^+ + OH^- \text{ or } H_2O_2 \rightarrow \bullet OH \quad (26)$$

$$e^- + O_2 \rightarrow \bullet O_2^- \quad (27)$$

$$\bullet OH + \frac{EBT}{MB}\text{dye} \rightarrow x\,CO_2 + yH_2O + \text{biproduct} \quad (28)$$

Where x and y are the stoichiometric number of carbon (IV) oxide and water molecules respectively.

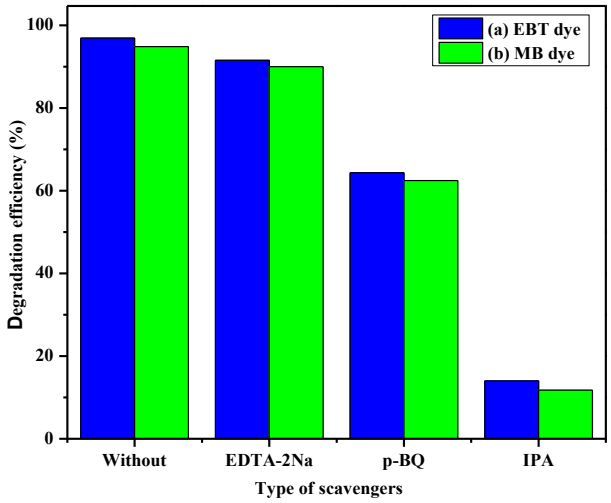

Figure 15. Photocatalytic degradation of (a) EBT dye (b) MB dye in the presence of scavengers and absence

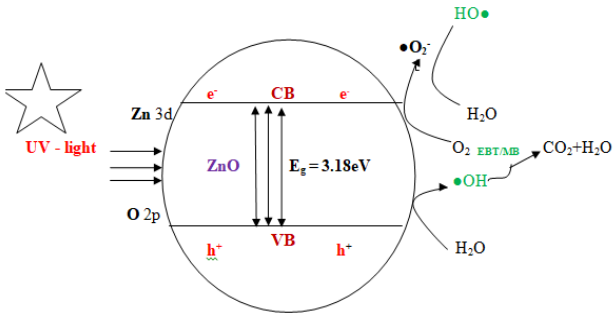

Figure 16. Mechanism of the photocatalytic degradation of EBT and MB Dyes over ZnO photocatalyst

3.2.8 Durability test

To determine the stability, durability and reusability for the synthesized ZnO photocatalyst, number of experiments were conducted at the optimum conditions of the photocatalytic degradation of EBT and MB dyes over the TiO_2 NPs. Residual catalyst from degradation experiment

was filtered, washed and dried and then recycled in fresh experiment and the result is illustrated in Figure 17. From the Figure 17, it can be seen that the degradation of eriochrome black t decreased steadily from the 1st (95.75 %) and 2nd (94.93 %) cycles but 3rd (94.81 %), 4th (94.80 %), 5th (94.80 %) and 6th (89.99 %) cycles remained almost the same. Similarly, for the photocatalytic removal of methylene blue decreased from the 1st (94.75 %), and 2nd (93.93 %) cycles while the 3rd (93.93 %), 4th (93.80 %), 5th (93. 80%), and 6th (93.79 %) cycles also remained almost the same. This clearly indicated that the stability and effectiveness of the biosynthesized ZnO photocatalyst in the degradation of eriochrome black t and methylene blue dyes. These findings were in line with the study recorded by Auwal *et al* [41] and Behailu *et al* [75].

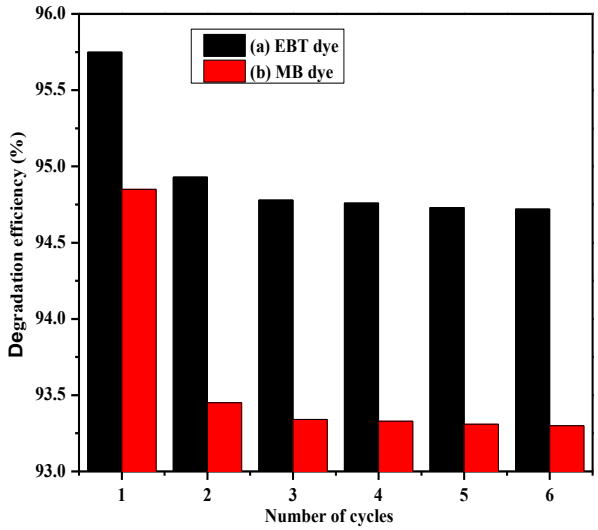

Figure 17. Reusability test of biosynthesized ZnO NPs for the photocatalytic degradation of (a) EBT dye (b) MB dye

3.3 Kinetic scheme

The kinetic of the photocatalytic removal of EBT and MB dyes using ZnO photocatalyst were investigated at optimal conditions of EBT/MB initial concentration, initial pH, initial temperature, and amount of ZnO photocatalyst under UV light. Three integrated kinetic models such as pseudo-zeroth, pseudo-first and pseudo-second order schemes were tested. However, the photocatalytic removal of both EBT and MB over the bionanosized ZnO photocatalyst were fitted the pseudo-first order kinetics with the coefficient of regression of R^2 = 0.9923 & 0.9972 respectively and the result is displayed in Figure 18. The apparent kinetic parameter known as velocity constant and coefficient of regression (R^2) for the photocatalytic removal of EBT and MB over the developed ZnO NPs according to the pseudo-zeroth, pseudo-first and pseudo-second order kinetics is shown in Table 9. It can be seen from the Table 9 that the apparent rate constant according to the pseudo-zeroth, pseudo-first order and pseudo-second order models were found to be 4.34 x10^{-2} moldm^{-3} s^{-1} & 3.21 x10^{-2} moldm^{-3} s^{-1} , 5.33 x10^{-2} s^{-1} &4.91 x10^{-2} s^{-1} and 3.73 x10^{-2} mol^{-1}dm^{3}s^{-1} & 2.97 x10^{-2} mol^{-1}dm^3 s^{-1} for the degradation of EBT and MB dyes respectively. While the coefficient of regression in accordance with the pseudo-zeroth, pseudo-first order and pseudo-second order models were found to be 0.8995 & 0.9123, 0.9923 & 0.9972 and 0.8321 & 0.8542 for the EBT and MB dyes degradation respectively. However, the highest value of coefficient of regression, R^2 (0.9923 & 0.9972) which are close to one (1) is a primary indication that the kinetic study for the photocatalytic degradation of EBT and MB using ZnO photocatalyst were followed the pseudo-first order kinetic model.

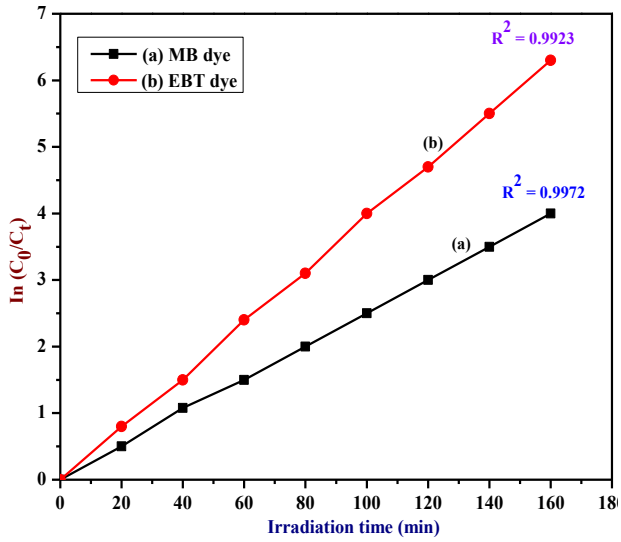

Figure 18. Pseudo-first order plot for the photocataltytic degradation (a) methylene blue (b) eriochrome black t using biosynthesized ZnO NPs under UV light irradiation

Table 9: Apparent rate constant (k_{app}) and coefficient of regression (R^2) according to the pseudo-zeroth, pseudo-first and pseudo-second kinetic for photo removal of EBT and MB dyes over ZnO NPs

S/NO	Dye	Model	Apparent rate constant (k_{app})	Correlation coefficient (R^2)
1	EBT	Pseudo-zeroth order	4.34 x10^{-2} moldm^{-3} s^{-1}	0.8763
		Pseudo-first order	5.33 x10^{-2} s^{-1}	0.9923
		Pseudo-second order	3.73 x10^{-2} mol^{-1}dm^3 s^{-1}	0.8321
2	MB	Pseudo-zeroth order	3.21 x10^{-2} moldm^{-3} s^{-1}	0.9123
		Pseudo-first order	4.91 x10^{-2} s^{-1}	0.9972

Pseudo-second order	2.97 x10^{-2} mol^{-1}dm^3 s^{-1}	0.8542

3.4 Thermodynamic investigation

The thermodynamic study of the photocatalytic degradation of eriochrome black t and methylene blue dyes using ZnO nanoparticles was investigate by carried out the photocatalytic experiments at different initial temperature such as 30.00, 40.00, 50.00, 70.00 and 90.00 ℃ while all other reaction conditions such as initial EBT/MB concentration, catalyst loading, initial pH were kept constant. The apparent rate constant (k_{app}) at each temperatures for the degradation of EBT and MB dyes were calculated using Equation 2 and the results obtained are presented in Figure 18. Accordingly, the k_{app} at each of the working temperatures for the photocatlytic removal eriochrome black t and methylene blue dyes were illustrated in Figure 18 (a) and (b) respectively. The activation energy (E_a) for degradation of EBT and MB dyes over ZnO NPs were evaluated using Equation 5 and the result was obtained is displayed in Figure. 19 (c). It can be seen that from the Figure 19 (c) the activation energy for the removal of EBT and MB dyes were found to be + 14.65 and + 8.94 kJ mol^{-1} respectively. Positive sign of E_a indicated that the photoreactions for EBT and MB dyes removal are endothermic processes. But the E_a for the MB removal is lower than that of the EBT removal and thus the reaction is more facilitated in the case of MB removal because of the lowering the catalyst. While the enthalpy and entropy change for the photoremoval of EBT and MB dyes were obtained using Equation 7 and the result was presented in Figure 19 (d).

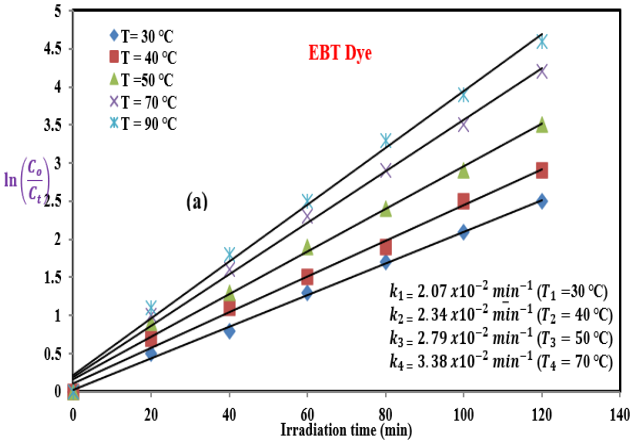

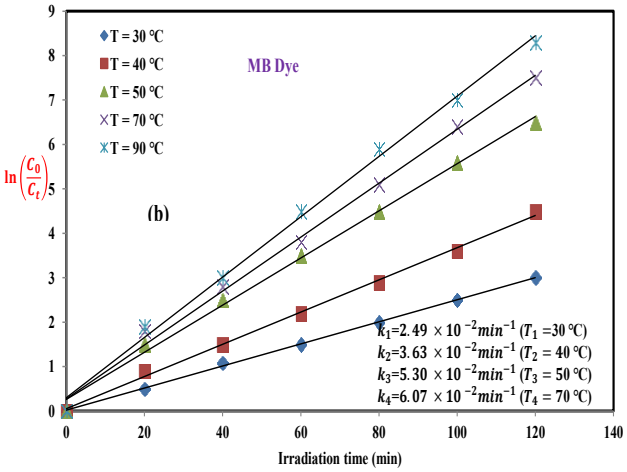

Figure 19. Pseudo-first order plot for the photocatalytic degradation (a) eriochrome black t dye (b) methylene dye using ZnO nanoparticles

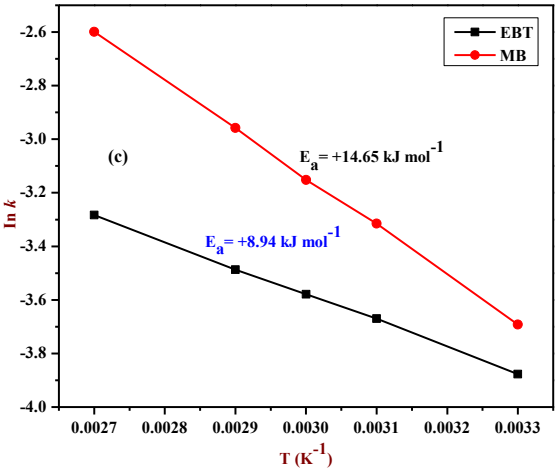

Figure 19 (c). Arrhenius plot of the photocatalytic removal of EBT and MB dyes over ZnO NPs

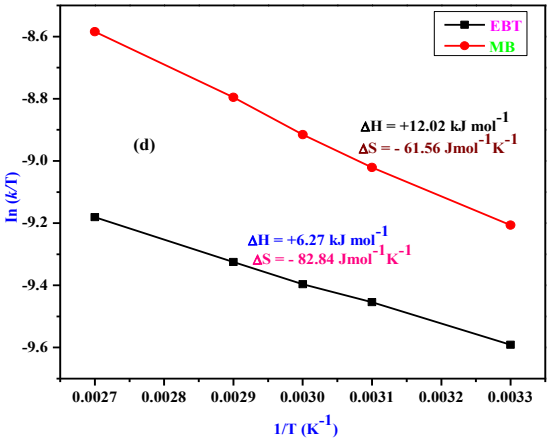

Figure 19 (d). Eryring Plot of the photocatalytic degradation of EBT and MB dyes using ZnO NPs

According to the Fig. 18 (d) the enthalpy and entropy change for the photocatalytic degradation of EBT and MB dyes were found to be + 6.27 and +12.02 kJ mol^{-1} and - 82.84 and - 61.56 $Jmol^{-1}K^{-1}$ respectively. Moreover, the enthalpy change and Gibbs free energy change at various temperatures were obtained using Equation 6 and 8 respectively. The results obtained are shown in Table 10

Table 10: Thermodynamic functions for the photocatalytic degradation of EBT and MB dyes over ZnO NPs at various temperatures according to Arrhenius plot

Dye	T (K)	E_a (kJ mol^{-1})	ΔH (kJ mol^{-1})	ΔS (J mol^{-1} K^{-1})	ΔG (kJ mol^{-1})
	303		+6.42	-258.17	+84.65
	313		+6.34	-257.39	+86.90
EBT	323	+8.94	+6.26	-256.21	+89.02
	343		+6.09	-255.12	+93.59
	363		+5.92	-254.96	+98.47
	303		+12.13	-256.58	+89.87
	313		+12.05	-253.77	+91.48
MB	23	+14.65	+11.96	-250.82	+92.97
	343		+11.79	-250.24	+97.62
	363		+11.63	-249.74	+102.29

Table 11: Summary of thermodynamic quantities for the photocatalytic degradation of EBT and MB dyes over ZnO NPs according to the Eryring plot

Dye	E_a (kJ mol^{-1})	ΔH (kJ mol^{-1})	ΔS (J mol^{-1} K^{-1})	ΔG (kJ mol^{-1})
EBT	+8.94	+6.27	-82.84	+31.37
MB	+14.65	+12.02	-61.56	+30.67

It can be seen from the Table 10 that the positive value of ΔH decreases as the temperature increases for both EBT and MB dyes indicated the endothermic nature of the catalytic process respectively. Similarly, the negative value of ΔS and positive value of ΔG increases as the temperatures increases for both EBT and MB dyes demonstrated that both the photocatalytic removal of EBT and MO dyes were non-spotaneous in nature. On the other hand Table 11 indicated that the E_a (+8.94 kJ mol^{-1}**)** of EBT is lowered than the E_a (+14.65 kJ mol^{-1}**)** of MB. This suggested that the catalyst lowered the activation barrier needed for the photocatalytic removal to occur. Based on these, the photocatalytic removal of EBT dye over ZnO NPs is less endothermic in nature as compared to that of the photoremoval of MB dye. Moreover, the ΔG of +31.37 and +30.67 kJ mol^{-1} obtained for EBT and MB dyes respectively also highlighted the non-spontaneous nature of the photoremoval processes. But EBT removal process exhibited a better non-spontaneity as compared to that of the MB removal. These findings were in line with results reported by Siddique *et al* [76].

3.5 Comparison

To demonstrate the research gap of the present photocatalytic degradation of eriochrome black t and methylene blue dyes over ZnO photocatalyst under UV light irradiation, the results obtained in this work were compared with the previous related works reported in the relevant scientific literature and the result is shown in Table 12. However, the Table 12 was presented in term of photocatalyst used, type of extract used, type of dye used, degradation efficiency and thermodynamic study during the photocatalytic reactions. It was observed from the Table 12, that the photocatalytic degradation of EBT and MB using ZnO nanoparticles under UV light irradiation exhibited in better degradation efficiency of 98.95 & 98.51 % respectively in 120 min on comparison with the previous related works recorded in the literature. This demonstrated that the biosynthesized ZnO NPs of the current study could be effectively used for the photoremoval of both EBT and MB dyes under UV light irradiation from the aqueous environment

Table 12: Comparison of the photocatalytic degradation of EBT and MB dyes for this work and previous related works reported in the relevant scientific literature.

S/NO	Catalyst	Extract used	Dye used	Degradation efficiency (%)	Thermodynamics	Ref
1	ZnO	*Justicia adhatoda*	MG	96.5	Not available	[77]
2	ZnO	*Pineapple skin*	CR	97.08	Not available	[43]
3	ZnO	*Carissa macrocarpa*	MB and MO	82.2 (MB) and 87.5 (MO)	Available	[76]
4	ZnO	*Passiflora foetida*	MB and RhB	93.25 (MB) and 91. 06 (RhB)	Not available	[42]
5	ZnO	*Eucalyptus leaves*	Acid black 210	62	Available	[78]
6	ZnO	*Padina pavonica*	MB	98	Not available	[44]
7	ZnO	*Jujube fruit*	MB and ECBT	92 (MB) and 86 (ECBT)	Not available	[79]
10	ZnO	Olea europaea	EBT	92	Not available	[80]
11	ZnO	*Brassica oleracea*	MB	80	Not available	[81]
12	ZnO	*Salvia officinalis*	MO	92.47	Not available	[82]

13	ZnO	*Elettaria cardamomum pod*	MG	99.8	Not available	[83]
14	ZnO	*Leonotis ocymifolia*	MB	89.81	Not available	[84]
15	ZnO	*Myristica fragrans*	MB	88	Not available	[85]
16	ZnO	*Cocos nucifera*	MB	84.29	Not available	[86]
17	ZnO	*Salvadora persica*	MO	68	Not available	[87]
18	ZnO	*Lychee peel*	CR	98	Not available	[88]
19	ZnO	*Acalypha indica*	MB	96	Not available	[89]
20	ZnO	*Vigna unguilculata L*	EBT and MB	98.95 (EBT) and 98.51 (MB)	Available	This work

.

4. CONCLUSİON

The present study successfully synthesized ZnO nanoparticle by using *Vigna unguiculata L*. extract as a reducing and stabilizing agent via co-precipitation method. The TG-DTA analysis revealed that the calcination temperature of ZnO was found to be 600 ℃. Thus the decomposition reaction of precursor during the biosynthesis of the catalyst is endothermic and non-spontaneous processes. The lattice parameters confirmed that the developed ZnO photocatalyst was matched to the standard hexagonal wurtzite ZnO nanoparticles. However, the band gap (3.18 eV) obtained for the developed ZnO was consistent with that of relevant scientific literature. Furthermore, the eriochrome black t and methylene blue dyes photocatalytic degradation under ultraviolet irradiation exhibited degradation efficiencies of 98.05 and 97. 51 % respectively in 120 min.. Radical scavengers test revealed that the •OH contributed more significantly during the photocatalysis. Moreover, the reusability test showed a good stability and durability for the developed ZnO nanoparticles. Additionally, the crucial and essential functions such as E_a, ΔH, ΔS and ΔG of the photocatalytic removal for both EBT and MB dyes over ZnO NPs under UV light irradiation indicated the endothermic and non-spontaneous in nature. But the photocatalytic removal of EBT exhibited less endothermic and non-spontaneity on comparison with that of the MB degradation process. Therefore, the synthesized ZnO nanoparticles could be effectively used for the photocatalytic degradation of eriochrome black t, methylene blue and other industrial effluents under UV light illumination.

ACKNOWLEDGEMENTS

The authors wish to thank Department of Chemistry Faculty of Physical Sciences, Federal University Dutsin-Ma for providing most of the facilities used in this research work.

DATA AVAILABILITY STATEMENT

The authors of this manuscript include all graphics and data collected during the study.

CONFLICT OF INTEREST

The authors declare that they have no potential conflicts of interest regarding the research, authorship and/or publication of this article.

USE OF AI FOR WRITING ASSISTANCE

The authors declare that they have not used the AI for writing of this manuscript

ETHICS

The authors of this manuscript stated that that there were no ethical issues in publishing

REFERENCES

1. M. Abdu, S. Tibebu, S. Babaee, A. Worku, T. A. M. Msagati, J. F. Nure, *Res. Eng,* 25 (2025), 104036. DOI: https://doi.org/10.1016/j.rineng.2025.104036
2. D. Raoufi,. *Ren Ener*. 5(2013), 932-937.
3. V. K. Savaranan, V. Gupta, A. Narayan, *J .Photochem .Photobio*. 181 (2013), 133-141.
4. A. Sarith, H. Shank, T. Prakash, C. Sampa, *J. Hazar Mater,* 45(2017), 335-340.
5. S. Supamas, S. Schrank, P. Josa, Y. T. Hiranok, *J. Photochem. Photobio*.; 34 (2014), 225-258.
6. O.O.C. Maureen, O.J. Nnaemeke,N. A. Basil, E. O. Emeka, *Inter.Lett .Chem, Phy . Astron.*, 81 (2019), 18-26.
7. X.W. Chen, L. Danden, G. Zhen, *Nanoscal. Resear. Letts*, 2 (2017), 12-13.
8. M. Kian, S. Lee, B. Abdulhamid, and W. China, *J. Nanotechnol . Cataly. Resear Centr*, 42 (2015), 102-112.
9. A. Saka, Y. Shifera, K. Rmaswamy, *Sci. Rep*, 12 (2022), 15960. DOI: https://doi.org/10.1038/s41598-022-19440-w
10. M. Khadaic, N. Ghasemi, B. Moradi and M. Rahimi, *J. Chem*, 10 (2013), 383985
11. R. Thomas, W.N. Kingham. *W. Environ. Resear*, 64 (1992), 200-203. https://doi.org/10.217/WER.64.3.2.
12. Y.N. Teixeira, F.J.P. Filho, V. P. Bacurau, J. M. C. Menezes, A. Z. Fan, R. P. P. Melo, *Heliyon*, 8 (2022); e10868.
13. K. El-Moustaqim, B. El-Bakraoui, J. Mabrouki, L. T. Igbigbi, *Sustainability*, 15 (2023,), 16110. DOI: 10.3390/su152216110

14. D. Abdessemed, G. L. Nezzal, B. R. Aim,, *Desalin*, 126 (1999), 1-5. DOI: 10.1016/S0011-9164(99)0049-6
15. S. N. Ahmedzeki, S. Al-Jubouri, H. R. Salman, *J. Eng*, 15 (2009), 4356. DOI: 10.31026/j.eng.2009.04.17
16. H. Eslami, S. S. Khavidak, F. Salehi, R. Khosravi, R. Fallahzadeh, R. Peirovi and. S. Sadeghi, *J. Adv. Environ. Health Resear*, 5 (2017), 10-15.
17. M. Z. A. Alaizeri, A. H. Alhadlaq, S. Aldawood, and A. Y. N. Abduh. *RSC Adv*, 14 (2024), 16685.
18. M. F. Lanjwani, Y. Muhammad, T. Khuhawar, J. Khuhawar, A. Lanjwani, S. Q. Memon, W. A. Soomro, I. K. Rind, *J. Clus. Sci,* 23 (2022), 293-8.
19. A. Jurex, X. Zheng, Z. Zhai, Q. Zhao, *J. Photochem.Photobiol, RSC*, 31(2012), 111-118.
20. J. Zhang, D. Fu, Y. Xu, C. Liu, *J. Hazar. Environ. Sci*, 22 (2010), 1281-1289.
21. M. Z. B. Mukhlish, F. Najnin, M. M. Rahman, M. J. Uddin, *J. Scient. Resear*, 5 (2013), 301-314
22. M. F. H. Abd El-kader, M. T. Elabbasy. A. A. Adeboy, G. M. M. Zeariya, A. A. Menazea, *Elsevier B.V*; 10 (2021), 2238-78454
23. Y. Ibrahim, H. M. Isah , A. K. Aminu, A. Abubakar, *Niger. Resear J Chem. Sci*, 8 (2020), 328-338.
24. K.P. Sridevi, S. Sivakumar, B. Sangeetha, K. Seravann, H. Praveen, *Nat Vol .Essen. Oil,* 8 (2021): 4840-4853.
25. R. Qin, F. Meng, M. W. Khan, B. Yu, H. Li, Z. Fan, and J. Gong, *Mater. Letts,* 240 (2019), 84-87
26. A. Weir, P. Westerhoff, L. Fabricius, K. Hristovski, N. Von Goetz. *Environ Sci Technol* 2012;46:2242e50.
27. P. Prasannalakshmi, N. Shanmugam, *Sci Semi Pro,* 61 (2017), 114–124.
28. G. K. Upadhyay, J. K. Rajput, T. K. Pathak, V. Kumar, L. P. Purohit. *Vacuum,* ;160 (2019), 154–63.
29. A. Mazabuel-Collazos, C. D. Gómez, J. Rodríguez-Páez, *Mater Chem Phys*, 222 (2019), :230–45.
30. A. Y. Elderdery, A. H. Alhamidi, A. M. Elkhalifa, M. M. Althobiti, E. M. Tebien, N. E. Omer, *Green Process Synth.* 11(2022), 1026–39.
31. M. Lee, S. I. Han, C. Kim, S. Velumani, A. Han, A. H. Kassiba, *ACS Appl Mater Interfaces*.;14 (2022), 13801–11
32. Y. Auwal and U. I Gaya, *jphcfum*, 6 *(*2023)*)*,1-17. DOI: https://doi.org/10.54565jphcfum.1253804
33. A. Yusha'u, A.A Siaka, K. S Kabo, A. Muhammad, *Resear. Biotechnol Environ. Sci*, 2 (2023), 88-101. DOI: https://doi.org/10.58803/rbes.v2i4.32
34. Y. Rufai, S. Chandren, N. Basar. *Front. Chem*, 8 (2020), 597980. DOI: httsp://do.org.10.3389/fchem.2020.597980
35. J. Udayabhanu, V. Kannan, M. Tiwari, G. Natesan, B. Giovanni, V. Perumal.. *J. Photochem. Photobiol B. Bio*, 178 (2018), 496-504. DOI: https//doi.org/10.1016/j.photobiol.2017.12.005
36. K. A. Shimi, M. H. Ahmed, F. M. Wahab, S. Katheria., J. Nanomater, 2 (2022), 7060388, DOI: https;//doi.org/10.1155/2022/7060388
37. S. P. Jassal, D. Kaur, R. Prasad, J. Singh, J. *Agricul. Fo. Resear*, 3 (2022), *10*,10036 .DOI: https://doi.org/10.1016/j.jafr.2022.10035
38. V. Verma, M. Al-Dossari, M. Singh, M. Rawat, G. M. M. Kordy, M. A. Shaban, *Polym (Basel*), 14 (2022), 1444. DOI: 10.3390/polym14071444
39. A. Yusha'u, K. Abukaar, S. Darma, *Alger. J. Eng. Technol*, 8 *(*2023)*,*117-130. DOI: https://doi.org/10.57056/ajet.v8i1.100
40. Y. Auwal and U. I Gaya, *jphcfum*, 6 *(*2023)*)*,1-17. DOI: https://doi.org/10.54565jphcfum.1253804
41. Y. Auwal, S. K Kamal, M. Abdullahi, *jphcfum,* 6 *(*2023), 30-56. DOI: https://doi.org/10.54565jphcfum.1321022
42. M. Khan, P. Ware, N. Shimpi, *SN Appl. Sci,* 3 (2021), 6780
43. W. Setyarsih, L. Rohmawati, F. F. Ardiansyah, S.M. Marif, D. Darminto, *Tis Trends. Sci,* 22 (2025), 9042. DOI: https://doi.org/10.48048/tis.2025.9042
44. A. E. Alprol, A. Eleryan, T. M. Hamad, Sci. Rep, 14 (2024), 32160. DOI: https://doi.org/10.1038/s41598-024-80757-9
45. M. H. Kahsay, A. Tadesse, D. RamaDevi, N. B. Tadesse, *RSC Adv*, 9 (2019), 36967-36981. DOI: https://10.1039/C9RA07630A
46. R. A. Basit, Z. Abbasi, M. Hafeez, P. Ahmad, J. Khan, M. U. Khandaker, K. S. Al-Mugren, A. Khalid, *Crystals*, 13 *(*2023)*,* 281. DOI:10.3390/cryst13020281
47. S. M. Abegunde, E. F. Olasehinde, M. A. Adebayo, *Hybrid Adv*, 5 (2024), 100164. DOI: https://doi.org/10.1016/j.hybadv.2024.100164
48. Y. A. Selim, M. A. Azb, I. Ragab, M. Hm Abd El-Azim, *Sci. Rep*, 10 (1) (2020), 3445
49. G. Fuliang, C. Peng, W. Xiaoying, J. Kai, *Pro.Eng*, 43 (2012), 65-70. DOI; https://doi.org/10.1016/j.proeng.2012.08.012.
50. A. K. Shimi, H. M. Wahab, M. A. K. Snehlata, M. S. Wabaidur, E. G. Eldesoky, A. Islam, P. K. Md, Rane, *J. Nanomater*, 1 (2022), 7060388. DOI: https://doi.org/10.1155/2022/7060388
51. R. Dobrucka, *Iran J. Pharm.Res*, Springer, *16 (2*) (2017), 756-762
52. G. Nabi, W. Raza, B. M. Tahir, *J. Inorg.Organomet.Polym.Maters*, 2020, 1045. DOI: https://doi.org/10.1007/s10904-019.01248-3
53. A. AnsarI, U. V. Siddiqui, U. I. Rehman, K. Md. Akram, A. W. Siddiqi, M. A. Alosaimi, A. M. Hussein, M. Rafatullah, *Catal,* , 12 (2), (2022), 181. DOI: https://doi.org/10.3390/catal.12020181
54. W. Ahmad, K. K. Jaiswal, S. Soni,. *Inorg. Nano.Met.Chem*, 50 (2020), 1032-1038
55. N. A. Al-Shabib, F. M. Hussain, F. A. Qais, N. Ahmed, J. M. Khan, P. Alam, *Front.Microbio*, 11 (2020), 1-13
56. X. Wei, G. Zhu, J. Fang, J. Chen, *Inter J Photoenergy*, 1 (2013), 726872. https://doi.org/10.1155/2013/726872
57. T. Santhoshkumar, A. A. Rahuman, C. Jayaseelan, G. Rajakumar, S. Marimuthus, A. V. Kirthi, K.

Veloyutham, J. Thomas, J. Venkatesan, S-K. Kim, *Asian J. Trop. Med*, 7 (2014), 968-976
58. B. K. Thakur, A. Kumar, D. Kumar,. *Afr. J. Bot*, *124* (2019), 223-227
59. S. P. Jassal, D. Kaur, R. Prasad, J. Singh, J. *Agricul. Fo. Resear*, *10 (2022)*, 10036 .DOI: https://doi.org/10.1016/j.jafr.2022.10035
60. A. Saka, Y. Shifera, K. Rmaswamy, *Sci. Rep*, 12 (2022) ,15960. DOI: https://doi.org/10.1038/s41598-022-19440-w
61. K. Umar., and R. Adnan, *Key Eng. Maters*, *920* (2022), 36-42
62. A. Haghighizadeh , B. A. Ali , S. Farshad , *W. Air and Soi Pollut, 234* (366) (2023) ; 43-56
63. K.S. Saranya, T. P. Vellora, C. Senan, R. Pilan-Katta, K. Saranya, B. George, S. Wackawek, M. Cernik,. *Nanomater*, 8 (2018), 1002
64. S. Hussain, W. Nazar, A. Tajammal, Z. Nasreen, T. Ahmad, A. Asghar, Z. Mustafa, M. Shahidi, M. K. Batoo, S. Hussain, *Polym. J. Eviiron.Stud, 3* (2024), 2707-2714
65. M. Sundrarajan, S. Gowri, L. Chalcogenide, *Chalcogenide Lett*, *8 (2*) (2011), 447-451
66. S. Subhapriya, P. Gomathipriya, *Micro. Path*, *116* (2018), 215-220
67. R. Saini, P. Kumar, *Inorg. Chem. Comm*un, 156 (2023), 111221
68. A. M. N. Barakat, A. M. Kanjwal, S. I. Chronakis, Y. H. Kim, *J. Molec. Cataly A. Cheml*, *366 (2013)*, 333-340. https://doi.org/10.1016/j.molcat.2012.10.012
69. Y-W. Chen, Y-H. Hsu, *Catalysts*, *11* (2021), 966. https://doi.org/10.3390/catal11080966
70. S. P. Goutam, G. Saxena, V. Singh, A. K. Yadav, R. N. Bharagava, K. B. Thapa, *Chem. Eng. J*, *336 (*2018), 386-396
71. M. Abdu, S. Tibebu, S. Babaee, A. Worku, M. A. T. Msagati, F. J. Nure, *Result in Engineering*, 25 (2025), 104036. https://doi.org/10.1016/j.rineng.2025.104036
72. K. S. Kansal, S. Sood, A. Umar, S. K. Mehta, *J. Alloys. Compds, 581* (2013), 392-397. https://doi.org/10.1016/j.jallcom..2013.07.0169
73. S. Parra, E. S. Stanca, I. Guasaquillo, R. K. Thampi, *Appl. Catal. B: Environ*, *51* (2014), 107-116
74. A. Kumar, G. A. Pandey,. *Mater. Sci.Eng. Int. J, 1* (2017) 106-114
75. G. Behailu, T. D. Leku, A. G. Workneh, *ASC OMEGA*, 8 (2023), 43999-44012
76.] B. A Siddiqu, A. M. Shaheen, A. Abba, Rehman, Z. Zoghebi, K. Amin, M. A. H. Amin, *Heliyon*, 10 (2024), e40679
77. M. Mahajan, S. Kumar, J. Gaur, S. Kausal, J. Dalal, G. Singh, M. Misra, S. D. Ahlawat, *RSC.Adv*, 15 (2025), 2958-2980. DOI: 10.1039/D4RA08632E
78. A. Zahraa, M. Abdulmalik, A. K. Najah, A. Mohammad, Chemophere, 4 (2023), 3315. DOI: 10.33640/2405-609X3315
79. M. Golmohammadi, M. Honarmand, S. Ghanbari, *Spect. Acta. Part. A: Mol. Biomol. Spec,* 229(2020), 11796 DOI: https://doi.org/10.1016/j.saa.2019.117961
80. M. Thiam, A. J. Bernardo, V. O. A. Pellegrini, J. F. Possatto, Z. W. Dlamini, T. S. Mahule, B. D. Ngom, B. Q. Mosepele, F. T. Thema, B. B. Mamba, S. Vallabhapurapu, V. S. Vallabhapurapu, I. Polikarpov, *Processes*, 13 (2025), 880. DOI: https://doi.org/10.3390/pr13030880
81. U. Manojkumar, D. Kaliannan, V. Srinivasan, B. Balasubramanian, H. Kamyab, Z. H. Mussa, J. Palaniyappan, M. Mesbah, S. Chelliapan, S. Palaninaicker, *Chemosphere*, 323 (2023), 138263
82. M.M. Abomuti, E. Y. Danish, A. Firoz, N. Hasan, M. A.Malik, *J. Biology*, 10 (2021),1075. DOI: https://doi.org/10.3390/biology10111075
83. H. Kaur, A. Sharma, K. Anand, A. Panday, S. Tagotra, S. Kakran, A. K. Singh, M. W. Alam, S. Kumar, G. Bouzid, J. Dalal, G. Singh*, RSC. Adv*, 15 (2025), 16742-16765. DOI: https://doi.org/10.1039/D5RA01469G
84. D. Mutukwa, R. T. Taziwa, S. M. Tichapondwa, L. Khotseng, *Int. J. Mol. Sci,* 25 (2024), 11621. DOI: https://doi.org/10.3390/ijms25211162
85. S. Faisal, H. Jan, S. A. Shah, S. Shah, A. Khan, M. T. Akbar, M. Rizwan, F. Jan, Wajidullah, N. Akhtar, A. Khattak, S. Syed, *ACS Omega,* 6 (2021), 9709-9722. DOI: https://doi.org/10.1021/acsomega.1c00310
86. F. Rahman, Md. A. M. Patwary, Md. A. B. Siddique, M. S. Bashar, Md. A. Haque, B. Akter, R. Rashid, Md. A. Haque, A. K. M. R. Uddin, *RSOS,* 2022, 858. DOI: https://doi.org/10.1098/rsos.220858
87. S. A. Al Rahbi, A. H. Al Mawali, S. S. Al Rawahi, R. K. Al Dighishi, F. A. Al Abri, A. Ahmed, S. Rahman, *W. Pract. Technol,* 19 (2024), 1219-1231. DOI: https://doi.org/10.2166/wpt.2024.042
88. S. Jaishree, N. Singh, R. Singh, K. Shah, B. K. Pramanik, *Chemosphere,* 327 (2023), 138497. DOI: https://doi.org/10.1016j.chemosphere.2023.13849
89. G. Kamarajan, D. B. Anburaj, V. Porkalai, A. Muthuvel, G. Nedunchezhian, N. Mahendran, *J. Water. Environ. Nanochnol,* 7 (2022), 180-193. DOI: https://10.22090/jwent.2022.02.006